Charles University

Faculty of Science

Study program: Physical Geography and Geoecology

M.Sc. Theodora Lendzioch

UAV remote sensing of hydrological processes and fluvial dynamics

Dálkový průzkum hydrologických procesů a říční dynamiky pomocí UAV

Doctoral dissertation

Supervisor: Prof. RNDr. Jakub Langhammer, Ph.D.

Prague, 2023

To my parents and grandma

Declaration: I hereby declare that I have worked on the final thesis independently and reported all the data sources and literature used. This work has not been submitted to obtain any other academic title.

Prohlášení: Prohlašuji, že jsem závěrečnou práci zpracoval/a samostatně a že jsem uvedl/a všechny použité informační zdroje a literaturu. Tato práce ani její podstatná část nebyla předložena k získání jiného nebo stejného akademického titulu.

……………………
04.05.2023, Prague

Contents

ACKNOWLEDGEMENTS

Abstract

Using drones and machine or deep learning algorithms (ML or DL) for environmental monitoring offers several advantages over traditional methods, including gathering high spatial resolution data quickly and non-invasively, acquiring real-time data, and covering large and remote areas. This dissertation focuses on snow cover, river granulometry, river sustainability, river bathymetry, and peatland dynamics based on approaches of drone-based imagery that are critical for understanding fluvial processes in mid-mountain regions and their implications for streamflow patterns and ecosystem health. Measuring Snow Depth (SD) and vegetation characteristics like Leaf Area Index (LAI) accurately is essential for effectively predicting snow cover and snowpack persistence across study sites (papers I and III). A further aspect of the fluvial process mediator involves the reproducibility of drone data. This allows for seamless coverage of riverbeds and the determination of ideal parameters for sediment surface cover detection. This can be done through photo-sieving or DL technique, which can analyze Particle Size Distributions (PSDs) of an entire river point bar from top-view UAV images (as described in papers II and V).

Similarly, studying river sustainability with drones provides a unique opportunity to assess the effectiveness of stream restoration projects and inform management practices to ensure the long-term health and sustainability of fluvial systems (paper VI). Drone bathymetric data provide critical information about river channel morphology, sediment transport, and habitat availability (paper VII). Finally, studying peat bog complexes as an essential side component of fluvial processes makes accurate drone monitoring crucial for effective management and conservation efforts (paper IV). However, further research is necessary to apply these methods to other regions and ecosystems, as environmental conditions and characteristics can vary significantly across different locations.

Keywords: environmental research, UAV, UAS, drones, sensors, snow cover distribution, SD, LAI, CNN, DL, PSD, peatland dynamics, ML, groundwater level, soil moisture, river restoration, river bathymetry

Abstrakt

Bezpilotní systémy (UAV, drony) a algoritmy strojového nebo hlubokého učení (ML nebo DL) přinášejí do oblasti věd o Zemi kvalitativně nové možnosti pro monitorování životního prostředí a dynamických procesů v krajině. Jedná se zejména o schopnost rychlého a neinvazivního sběru dat s vysokým prostorovým rozlišením, kvalitativně širokou škálou senzorů, získávání dat v reálném čase, budování časových řad přesného monitoringu a pokrytí rozsáhlých a vzdálených oblastí. Tato disertační práce se zaměřuje na vybrané aspekty hydrologických procesů, kde je možné uplatnit potenciál UAV pro získávání kvalitativně nových informací o hydrologických procesech, ale i aspektech prostředí, ovlivňujících dynamiku odtoku a stav říčních ekosystémů v podmínkách změny klimatu a měnícího se prostředí. Jde konkrétně o monitoring sněhové pokrývky ve vazbě na charakteristiky disturbance lesa, dynamiku fluviálně-morfologických změn toků a jejich antropogenních změn nebo o dynamiku hydropedologických charakteristik rašelinišť, kde snímkování pomocí dronů přináší kvalitativně nové informace, zásadní pro pochopení dynamiky procesů a jejich změn v kontextu prostředí a ekosystémů.

Konkrétně stanovení výšky sněhu ve vazbě na charakteristiky zdravotního stavu lesní vegetace je významným kvalitativně novým vstupem pro porozumění procesům ukládání a tání sněhové pokrývky, umožňující jeho přesnější předpovídání v komplexním prostředí (články I a III). Přesný monitoring rozložení a změn teplotně-vlhkostních charakteristik horských rašelinišť, která významně ovlivňují variabilitu odtoku horských toků, dává možnost získat podrobné informace o reakci tohoto citlivého ekosystému na klimatické změny a zároveň přesněji predikovat dynamiku jejich hydrologického režimu (článek IV). Schopnost získávat bezešvé modely velmi vysokého rozlišení a reprodukovatelnost UAV monitoringu přinesla zásadní posun v možnostech analýzy fluviálně-morfologických změn říčních koryt. Práce představuje nové přístupy v několika směrech fluviálně-morfologikcých analýz. Konkrétně představuje novou metodu distribuce říčních sedimentů za využití vysoce podrobného UAV snímkování, kombinace optické granulometrie a využití technik hlubokého učení (DL) pro analýzu změn distribuce velikosti zrn v říční akumulaci ve vazbě na dynamiku říčního systému. Podrobné snímkování říčního koryta dále umožnilo ověřit možnosti batymetrické rekonstrukce koryt toků. Reprodukovatlenost UAV monitoringu pak umožnila získat informace o změnách hydromorfologických charakteristik a účinnosti projektů obnovy toků (příspěvek VI).

Práce přináší zhodnocení nových přístupů při aplikaci UAV snímkování pro analýzu fyzickogeografických procesů v měnícím se prostředí. Provedené studie zároveň ukazují na nezbytnost referenčích instrumentálních měření i dalšího výzkumu, zejména ve vazbě na proměňující se charakteristiky prostředí v důsledku klimatické změny a antropogenních tlaků na krajinu.

Klíčová slova: změny povrchu půdy, UAV, UAS, drony, hluboké učení, dynamika sedimentů, SD, tání sněhu, index opuštěných ploch, dynamika rašelinišť, hladina podzemní vody, půdní vlhkost, strojové učení.

List of publications included in the thesis

The thesis summarizes the results of seven papers published in well-recognized international Web-of-Science indexed journals attached as its Supplements.

Paper I

Lendzioch, T., Langhammer, J., & Jenicek, M. (2016). TRACKING FOREST AND OPEN AREA EFFECTS ON SNOW ACCUMULATION BY UNMANNED AERIAL VEHICLE PHOTOGRAMMETRY. *International Archives of the Photogrammetry, Remote Sensing & Spatial Information Sciences*, *41*. Vols. XLI-B1 (pp.917-923). https://doi.org/10.5194/isprs-archives-XLI-B1-917-2016

Author's contribution (80%): data collection, data processing, extensive literature research, statistical analysis, interpretation of results, drawing of figures, manuscript writing, and correspondence with the journal.

Paper II

Langhammer, J., Lendzioch, T., Miřijovský, J., & Hartvich, F. (2017). UAV-based optical granulometry as tool for detecting changes in structure of flood depositions. *Remote Sensing*, *9*(3), 240. https://doi.org/10.3390/rs9030240

Author's contribution (50%): statistical analysis, interpretation of results, drawing of figures, and manuscript co-writing.

Paper III

Lendzioch, T., Langhammer, J., & Jenicek, M. (2019). Estimating snow depth and leaf area index based on UAV digital photogrammetry. *Sensors*, *19*(5), 1027. https://doi.org/10.3390/s19051027

Author's contribution (80%): data collection, data processing, extensive literature research, statistical analysis, interpretation of results, drawing of figures, manuscript writing, and correspondence with the journal.

Paper IV

Lendzioch, T., Langhammer, J., Vlček, L., & Minařík, R. (2021). Mapping the ground-water level and soil moisture of a montane peat bog using UAV monitoring and machine learning. *Remote Sensing*, *13*(5), 907. https://doi.org/10.3390/rs13050907

Author's contribution (80%): data collection, data processing, extensive literature research, statistical analysis, scripting, interpretation of results, drawing figures, manuscript writing, and correspondence with the journal.

Paper V

Lendzioch, T., Langhammer, J., Sheshadrivasan, V.K. (2023). Using the CNN-based GRAINet model for automated mapping of grain size distributions from UAV imagery. *Remote Sensing*, (*under review*)

Author's contribution (100%): data collection, data processing, extensive literature research, statistical analysis, scripting, interpretation of results, drawing figures, manuscript writing, and correspondence with the journal.

Paper VI

Langhammer, J., Lendzioch, T., & Šolc, J. (2023). Use of UAV Monitoring to Identify Factors Limiting the Sustainability of Stream Restoration Projects. *Hydrology*, *10*(2), 48. https://doi.org/10.3390/hydrology10020048

Author's contribution (25%): manuscript co-writing and editing.

Paper VII

Witek, M., Walusiak, G., Halicki, M., Remisz, J., Borowicz, D., Parzóch, K., Kasprzak, Ł., Langhammer, J., Gallay, M., Miřijovský, J., Šašak, J., Kaňuk, J., Lendzioch, T.,

Minařík, R., Popelka, S., Niedzielski, T., 2023. Reconstructing bed topography of a shallow river from close-range aerial imagery: multi-drone experimental campaign in the Izera river (SW Poland/N Czechia). International Journal of Applied Earth Observation and Geoinformation. IF 7.672 (*under review*)

Author's contribution (15%): data acquisition and processing DJI Matrice 210-RTK V2 data.

---

1. Scope and aim of the thesis

Environmental research necessitates interdisciplinary knowledge, which is critical for environmental scientists (Elliott et al., 2019) to establish systematic protocols for managing sensitive and incidental findings (Wolf et al., 2008). Unmanned Aerial Vehicles (UAV), Remotely Piloted Aircraft Systems (RPAS), and Unmanned Aerial Systems (UAS), which are commonly referred to as drones (e.g., multi-rotor, fixed-wing, hybrid), are powerful research instruments, providing a unique earth observation capacity across a large number of applications allowing researchers to obtain data more quickly, non-invasively, inexpensively, and safely than before (K. Anderson & Gaston, 2013). Despite technological advancements, challenges persist in acquiring high-quality data, underscoring the importance of standardized workflows. By merging on-site data collection (in-situ) with high-resolution drone observations, researchers can better comprehend and characterize phenomena at different scales in the landscape (Levin, 1992; Marceau, 1999; Turner et al., 1989).

Thus, this dissertation aims to investigate the potential of using drone sensing to collect diverse types of data, including commercial Red-Green-Blue (RGB), Multispectral (MS), and Thermal-Infrared (TIR) cameras, to enable high-quality drone-based data collection for various environmental processes. These processes include snow hydrology (papers I and III), river fluvial dynamics including granulometry (papers II and V), peat bog dynamics (paper IV), river restoration and sustainability (paper VI), and bathymetry extraction (paper VII). The complex and multifaceted interlinkages between these processes highlight the significance of drones for data collection in understanding and managing environmental systems.

The distinct unique properties of snow, such as high albedo of the surface, high latent heat of phase transition, and adiabatic effect, directly impact the intricate energy balance of the Earth's surface, making it a crucial component in shaping the climatic system and contributing to regional and global climate changes (Barnett et al., 1989; Kittel et al., 2011; Qin et al., 2021). To study these unique snow properties and finely estimate snow parameters (Rekioua et al., 2017), our research (papers I and III) utilizes UAV digital photogrammetry to map snow cover and its characteristics and investigate the impact of forest canopy metrics on snow accumulation and ablation in open and coniferous areas where Leaf Area Index (LAI) and canopy coverage significantly modulate snow processes, especially in the latter one. Accurate estimation of Snow Depth (SD) distribution (a snow metric) and retrieval of LAI (a forest metric) is crucial in explaining snowpack dynamics and their implications for streamflow patterns.

Fluvial river dynamics (e.g., Chen et al., 2019), including granulometry (i.e., the size distribution of sediment particles in a river) (papers II and V), are influenced by the water and sediment inputs from snowmelt and other sources. Changes in sediment transport can alter the river channel morphology and affect the habitat quality for aquatic biota (e.g., Beltaos & Burrell, 2021; Hauer et al., 2018; Tsyplenkov et al., 2023). Consequently, the motivation arose to research sediment monitoring using UAVs to map grain size and distribution along a river point bar floodplain in the upper Vydra basin, which has the potential to enhance our understanding of sediment transport processes and their impact on the river ecosystem. By testing new methodologies for coupling optical granulometric surveys with UAV imagery, we overcame the limitations of existing methods. We improved the reproducibility and accuracy of sediment surface cover detection. Additionally, using Convolutional Neural Network (CNN) algorithms for automatic mapping granulometry has provided a fully automatic method for estimating Particle Size Distribution (PSD) directly from image texture, allowing for detecting multitemporal changes in PSD over the entire gravel bar floodplain (paper V).

Alternately, peat bog dynamics can be influenced by the hydrological regime of the surrounding landscape, including the input of water and nutrients from rivers and other sources (Kizuka et al., 2023). Changes in river fluvial dynamics, such as altered water levels or sediment inputs, can affect the peat bog vegetation composition, nutrient cycling, and carbon storage (Battin et al., 2023). As a result, peat bog degradation can affect the water quality and quantity of the surrounding rivers and the habitat quality of the species that depend on the peatland ecosystem (e.g., Jones, 2023; Serafin et al., 2023). Therefore, the motivation for paper IV arose from the need to improve the ability to observe and understand hydrological processes and fluvial dynamics using UAV platforms and advanced techniques. This can help overcome the limitations of traditional fieldwork methods by investigating the correlation

between predictors and Groundwater Level (GWL) and the top-layer Soil Moisture (SM) and evaluating the ML model's performance in predicting reference data points, which contributes to understanding the processes and dynamics of hydrology and fluvial systems and helping to guide conservation and restoration efforts.

River restoration projects often aim to improve the natural fluvial dynamics and sediment regimes and involve interventions such as bank stabilization, channel realignment, or dam removal (e.g., Copeland et al., 2001; Grabowski et al., 2022; Mondal & Patel, 2022; Wyrick & Klingeman, 2011). The success and sustainability of such projects depend on the accurate assessment of the initial river morphology and sediment budget and the long-term monitoring of the restored system. Thus, the motivation for paper VI arose from the need to define hydromorphological indicators suitable for the reliable determination of quantitative and qualitative aspects of hydromorphological quality from optical UAV monitoring and to test the practical applicability of the proposed approach to other restoration projects. Using UAV monitoring with optical RGB sensors can be an effective and affordable way to gather spatial information to help assess the critical geometric and qualitative aspects of stream restorations. By merging this information with established hydromorphological assessment methods, it is possible to obtain more reliable, feature-rich, and consistent information on the effectiveness and sustainability of stream restoration projects. This approach can lead to better-informed decision-making regarding stream restoration projects and their ecological impacts.

Bathymetry extraction of shallow rivers can provide valuable information on the riverbed morphology, which is essential for understanding sediment transport and fluvial dynamics (Bandini et al., 2017; Carrivick & Smith, 2018; Szafarczyk & Toś, 2023). Accurate bathymetry data can also help design and assess river restoration projects' effectiveness. The method of bathymetry extraction can involve various techniques, including Structure-from-Motion (SfM) algorithms (Mishra et al., 2023). Therefore, the motivation for paper VII arose from the need to explore the effectiveness of different drone platforms in reconstructing river bathymetry under the same conditions. The repeatability and reproducibility of the UAV-SfM approach were also tested, and its robustness for bathymetry extraction was assessed. UAVs are prone to collect high-resolution data, whereas traditional survey methods may be difficult or expensive to implement.

In conclusion, this thesis presents promising proof-of-concept methods on UAV data-collection techniques, where future research is needed to develop these techniques further and apply them to multiple environments within different regions by improving model calibration and better estimates of future monitoring change detection in mid-mountain regions.

2. Interconnections of the cryosphere, fluvial geomorphology, and hydrological processes

The cryosphere, fluvial geomorphology, and hydrological processes are interconnected through various mechanisms and feedback loops. For instance:

1. *Cryosphere-Fluvial Geomorphology Interconnection:* The cryosphere, which includes frozen components of the Earth's surface such as glaciers, snow cover, and permafrost, can have a significant impact on fluvial geomorphology, which involves the study of river channels, floodplains, and other landforms shaped by water (Knight & Harrison, o. J.). For example, melting glaciers and snow cover can increase river runoff and sediment supply, influencing river channel morphology, sediment transport, and floodplain formation (e.g., Stigter et al., 2021; Suter & Hoelzle, 2002). Changes in cryospheric features can also affect water availability, the timing of runoff, and streamflow dynamics, which in turn can impact fluvial geomorphological processes such as erosion, deposition, and channel evolution (e.g., Bugmann et al., 2007; Knight, 2022; Leng et al., 2022).

2. *Cryosphere-Hydrological Process Interconnection:* The cryosphere plays a critical role in the hydrological cycle, which involves water movement in various forms, such as precipitation, runoff, evaporation, and condensation (Pagano & Sorooshian, 2002). Cryospheric components, such as snow and ice, act as reservoirs that store water and release it gradually during melting, affecting the timing and magnitude of runoff (Wever et al., 2014). Changes in cryospheric features, such as shrinking glaciers or reduced snow cover, can alter the hydrological processes

11

by affecting water availability, streamflow dynamics, and water quality. Additionally, cryospheric changes can impact regional and global climate patterns, influencing hydrological processes at larger scales (e.g., Fountain et al., 2012; Milner et al., 2017; Rasul & Molden, 2019).

3. *Fluvial Geomorphology-Hydrological Process Interconnection:* Fluvial geomorphology and hydrological processes are closely linked, as rivers and their associated landforms are shaped and influenced by water flow and sediment transport (e.g., Balasubramanian, 2010; Ferguson et al., 2022). River channels, floodplains, and other fluvial landforms are formed and shaped by the erosive and depositional processes driven by water flow, sediment supply, and vegetation dynamics (Ferguson et al., 2022). Changes in river flow regime, sediment transport, and channel morphology can, in turn, affect hydrological processes such as runoff, evapotranspiration, and water quality (e.g., Leopold & Wolman, 1957; SCHUMM & Khan, 1972). For example, alterations to river channels through human activities, such as channelization or damming, can impact hydrological processes and alter fluvial geomorphological dynamics (e.g., paper VI).

Hence, changes in one system component can have cascading effects on the others, influencing water availability, the timing of runoff, sediment transport, river channel morphology, and other related processes. Understanding these interconnections is essential for comprehensively studying and managing water resources, river ecosystems, and climate change impacts on the Earth's hydrological system. UAVs have provided an efficient and effective means for collecting high-resolution data in these areas, allowing for better insights and understanding of these processes.

2.1 Advancements in sensor technology and UAVs for cryospheric research: Revolutionizing snow cover mapping and monitoring

The advancements in sensor technology, such as low-cost micro-sensors and UAV availability, have revolutionized environmental research, particularly in cryospheric studies. These technologies have become integral to the cryospheric toolkit (Bhardwaj et al., 2016), allowing for the cost-effective, rapid, and flexible collection of high-resolution data at more minor regional scales (Rhee et al., 2017). Researchers previously relied on limited in-situ observations or sparse satellite-based Remote Sensing (RS) data to study environmental processes. However, using UAVs has opened up new possibilities for cryospheric scientists, providing a safer alternative to ground-based measurements in hazardous or remote snow-covered environments, such as avalanche-prone areas (Birkeland et al., 1995; Součková et al., 2022) or glacier margins (Narro Pérez et al., 2023; Sobolewski et al., 2023). This has enabled researchers to understand snow distribution and properties for various applications, including weather forecasting, hydrological modeling, avalanche forecasting, climate change research, and winter sports management.

Among the wide variety of sensors used in cryospheric studies, such as RGB, miniaturized Light Detection and Ranging (LiDAR), Multispectral (MS), or TIR cameras, optical imagery remains the primary data source, providing high-resolution and real-time data on snow properties, such as SD, which is the vertical distance between the top snow surface points and the top bare ground point. Researchers also use other sensors, such as those mentioned above, for data collection and interpretation, such as Snow Water Equivalent (SWE), snow density, snowmelt volume, and snowmelt timing, allowing for on-demand and real-time data acquisition and frequent and repeated measurements to capture snow cover dynamics and changes. Table 1 provides examples of snow cover mapping and monitoring methods and their vertical accuracies based on Digital Elevation Models (DEMs) or Digital Surface Models (DSMs) derived from elevation differences between snow and terrain surface compared to reference data.

UAVs are combined with other technologies like manual probing, magnaprobe (Sturm & Holmgren, 2018), or Ground Penetrating Radar (GPR; e.g., McGrath et al., 2019) to provide reference data. However, relying solely on sparse and biased point measurements may not capture the high variability of SD. Combining UAVs with Airborne Laser Scanning (ALS), Terrestrial Laser Scanner (TLS), or both offers unique advantages for snow mapping, allowing for comprehensive and high-resolution data capture from air or ground perspectives. However, integrating UAVs with LiDAR techniques, MS, TIR,

or Hyperspectral (HS) cameras presents challenges such as accurate georeferencing, data processing, storage requirements, and cost considerations. Moreover, these sensors are only sometimes consumer-friendly and require significant resources to ensure calibration accuracy and sufficient user training to extract usable and scientific information (Tmušić et al., 2020).

Table 1. Overview of different snow cover mapping and monitoring technologies and their vertical Snow Depth (SD) accuracies, spatial coverage, cost, advantages, and limitations, found in the literature.

Method	Vertical Accuracy (m)	Spatial Coverage	Cost	Advantages	Limitations	Publications
ALS*	0.1 - 5.0	Large areas	High	Accurate and comprehensive 3D models of snowpack, suitable for difficult-to-access areas	High cost of sensors	Currier et al., 2019; Deems et al., 2013; Mazzotti et al., 2019, 2020; Painter et al., 2016
TLS**	< 0.10	Up to 1000 m	Moderate	Accurate measurements of SD, suitable for smaller areas	Limited spatial coverage compared to ALS	Prokop, 2008; Prokop et al., 2008
Satellite-based Imagery (Pleiades)***	0.47 - 1.47	Moderate to large areas (>100 km²)	Moderate	Provide high-resolution imagery, relatively lower cost compared to LiDAR technologies	Lower spatial resolution, which results in reduced vertical accuracy, costly, GCPs necessary	Deschamps-Berger et al., 2020; Eberhard et al., 2021; Marti et al., 2016
UAV-based Photogrammetry ****	0.1 - 0.16	Vast areas	Low	High spatial resolution and accuracies	Relying on weather conditions, limited payload capacity	Avanzi et al., 2017; Bühler et al., 2016; Cimoli et al., 2017; De Michele et al., 2016; Eberhard et al., 2021; Vander Jagt et al., 2015
Direct Georeferencing (UAV)*****	(<0.10)	Vast areas	Low	Lower accuracy compared to ground control-based UAV surveys	Snow process at local measurement scales	Vander Jagt et al., 2015

*Either compared to TLS ground-based data, GPS-equipped magnaprobe or manual snow probing, **Compared to manual snow probing or tachymetry survey, ***Compared to UAV snow maps and terrestrial imagery, ****Compared to manual snow probing, MultiSation scan or UAV snow maps. *****Direct georeferencing without Ground Control Points (GCPs).

Another possibility is integrating satellite data, enabling multi-sensor data fusion (e.g., Eberhard et al., 2021). However, some challenges and considerations exist when integrating UAVs with satellite data for snow cover monitoring. It requires careful data processing and integration (e.g., geometric and radiometric corrections, co-registration, and data fusion from different sensors and platforms), cost and logistics (e.g., equipment, personnel, logistics, and data storage), regulatory and operational aspects (e.g., permissions and permits), data continuity and reliability (e.g., adverse weather conditions or limit of UAV data). The standalone use of RGB-based imagery is adequate to get high-resolution snow cover maps (mm to m resolution) while delivering valuable outputs (papers I and III). However, each platform has advantages and disadvantages and must overcome challenges such as steep terrain (high parallax),

sensor saturation due to high-albedo surfaces, and poor stereo-correlation in limited surface texture for fresh snow (Eberhard et al., 2021). While UAVs have demonstrated an improved understanding of snow distribution in heterogeneous landscapes in certain studies (e.g., papers I and III), additional research is required to enhance accuracy and expand coverage.

2.2 Advancements in UAV remote sensing techniques for river morphology monitoring and grain size estimation: A focus on image-based methods and deep learning approaches

Observing rivers repeatedly is crucial for understanding flood events and river morphology. However, traditional methods like ALS or airplane photogrammetry are expensive and inflexible (Lane et al., 2000, 2010; Legleiter, 2012), while TLS is limited to smaller areas (Brasington et al., 2012). Satellites have limitations in accuracy due to coarse spatial resolution. Traditional granulometry methods involve laborious field measurements (e.g., Fehr, 1987; Wolman, 1954). Therefore, there is a need for more flexible and cost-effective methods to monitor and study rivers. Researchers have turned to image-based methods for grain size estimation to reduce effort and potential biases. These methods have been popular since the early 2000s and have recently been extended to quantify grain size using UAVs and low-cost photogrammetry software. Studies by Carbonneau et al. (2018), Detert & Weitbrecht (2012), and (Purinton & Bookhagen, 2019) have shown promising results in reducing manual data collection time and effort and minimizing biases associated with traditional methods. Paper II has successfully utilized UAV orthomosaics and implemented the approach after Detert & Weitbrecht (2012) based on the representative segmentation approach, where individual grains are identified through image segmentation to extract precise grain size information from targeted transects of fluvial gravel bars, showing that this method expands the area of investigation beyond the traditional local sampling approaches. However, this approach has limitations due to overlapping or irregularly shaped grains and vegetation or shadows in the images (Mair et al., 2022).

To overcome this, recent advancements in DL frameworks have enabled remote grain size measurements from scaled or georeferenced UAV images, eliminating the need for time-consuming field calibration. One promising DL approach, as demonstrated by Lang et al. (2021), is based on the digital line sampling technique and utilizes CNNs to analyze UAV datasets one-to-one, resulting in improved accuracy and precision of grain size measurements. This presents a promising solution to the challenge of grain size estimation (paper V). DL approaches can revolutionize how grain size and other parameters are measured in RS applications, reducing the potential for human error and increasing data collection and analysis efficiency, which can facilitate the study of various geological and environmental phenomena (paper V).

Furthermore, integrating the capabilities of UAV optical imagery and photogrammetric reconstructions with established digital image analysis and hydro-morphological assessment methods can enhance the availability, quality, consistency, and reproducibility of information related to stream restoration effectiveness and sustainability (paper VI), as well as river bottom information extraction and reconstruction (paper VII).

2.3 Assessing peatlands with UAV remote sensing: Monitoring hydrological dynamics

Peatlands are considered significant ecosystems threatened by various factors, including climate change, land use changes, and drainage for agriculture or industrial purposes. These ecosystems are vital in regulating the hydrological cycle and storing carbon, which makes them critical in mitigating the effects of climate change (Grabowski et al., 2022). UAVs can help map and monitor these ecosystems, providing essential data on their health, hydrological dynamics, and carbon storage potential, which are critical for effective conservation and management strategies (Dinsmore et al., 2008; Harris & Baird, 2019). Understanding the rate at which the peat environment responds to disturbances is necessary to accurately assess the future fate of peatlands (Loisel et al., 2014, 2021). As for the other studies in this dissertation, UAV RS provides exciting new capabilities for peatland observation. The groundwater table is commonly characterized as GWL - defined as the height of groundwater above mean sea level - and Depth-to-Water (DTW) - the groundwater depth relative to local terrain level. These two metrics are related. The groundwater is typically measured reliably in the field using point-based techniques such as piezometers or shallow monitoring wells (paper IV), which are difficult to install and require repeated

field monitoring. Alternatively, GWL and DTW can be estimated via UAV-derived products, as done by Lovitt et al. (2018).

The water content in the soil, known as SM, plays a vital role in controlling decomposition rates and affecting carbon balance (Turetsky et al., 2015). SM is characterized as the water content available for plant metabolism (Ahmed et al., 2017), influencing diversity patterns (Xu et al., 2018), and ecosystem features (Damm et al., 2022). It also affects drought stress (Liu et al., 2021), vegetation distribution (Orru et al., 2016), microbial activity (Fenner & Freeman, 2011), disturbance proneness (Grau-Andrés et al., 2019), and carbon cycling balances (Kimmel & Mander, 2010; Sharma et al., 2022) — variations in water availability impact peatlands' ability to absorb or emit greenhouse gases (Nijp et al., 2017). Different approaches are used to obtain SM data to understand better and monitor water availability in peatland ecosystems. Three approaches are commonly used to measure SM in peatland ecosystems: in-situ measurements, physically based predictions, and RS. In-situ measurements involve collecting samples from specific points, providing precise, time-consuming, and expensive data that may not capture total variability (Silva et al., 2023). Physically based predictions use models to represent ecosystem processes and structures, providing a comprehensive view but requiring accurate input data and assumptions (Grayson et al., 1992a, 1992b). RS predictions use satellite or ALS data to measure SM over a large area but have lower spatial resolution and accuracy and are limited to the top few centimeters of soil (<5 cm) (Brocca et al., 2017). RS methods like ground-penetrating radar or cosmic-ray neutron probes provide information on deeper SM but also have limitations. In some cases, in-situ measurements are preferred for their accuracy, despite being limited to small scales (Rahimzadeh-Bajgiran et al., 2013; Wigmore et al., 2019).

Machine Learning (ML) algorithms such as Random Forest (RF) and Extreme Gradient Boosting (XGBoost) are increasingly used in soil and water science research (Malekzadeh et al., 2019; Naghibi et al., 2017; Salehi Hikouei et al., 2021). These algorithms have been recognized as powerful tools for technological progress, particularly in monitoring and predicting different characteristics of groundwater resources. ML models are practical and efficient in modeling various environmental variables (Raghavendra & Deka, 2016; Regan et al., 2019). Recent research has also demonstrated the potential of ML algorithms in classifying different peatland microforms using drone imagery and exploring the extent to which changes in this microform are related to climate and land-use drivers (Steenvoorden et al., 2022). However, there is still a knowledge gap in understanding how these algorithms could be applied to model GWL and SM in peatlands based on reference sample points, especially at different temporal and spatial scales. The combination of ML algorithms with UAV multisensor data has the potential to provide precise monitoring tools at a low cost, as demonstrated by paper IV. This approach provides a more comprehensive understanding of peatland hydrology and aid in developing management strategies to protect and restore these valuable ecosystems. Nevertheless, further research is needed to explore the potential of these algorithms to model GWL and SM in peatland and to comprehend the implications of different temporal and spatial scales.

2.4 Platforms and sensors

The optimal platforms and sensors for a survey hinge on various factors, including spatial and spectral resolution, aerial coverage, and image quality requirements. Additional considerations may include available time and budget. The primary challenge lies in determining the suitable platform and sensor design, encompassing desired spatial coverage, ground resolution, and spectral resolution (Tmušić et al., 2020).

2.4.1 UAV platforms

UAVs are classified based on weight, endurance, altitude, and operational radius, with differences in size, cost, and payloads. The most commonly used UAVs in environmental studies are rotary-wing, fixed-wing, or hybrid UAVs (Figure 1a,b,c,d), selected according to study objectives, necessary payload, flight ranges, maneuverability requirements, and similar factors. Multi-rotor drones (Figure 1a, b) have high agility and maneuverability, vertical takeoff and landing, but lower flight speeds and altitude due to rotor energy requirements, making them preferable for environmental mapping. Fixed-wing UAVs (Figure 1c) offer longer endurance, greater payload capacity, and higher flight speed, but image quality

might be poorer due to the prone to blurry images (e.g., motion blur). Hybrid UAVs (Figure 1d) use electric motors/rotors for Vertical Takeoff and Landing (VTOL) and wings for horizontal and level flights powered by electric or internal combustion engines. However, Hybrid drones are still associated with high costs.
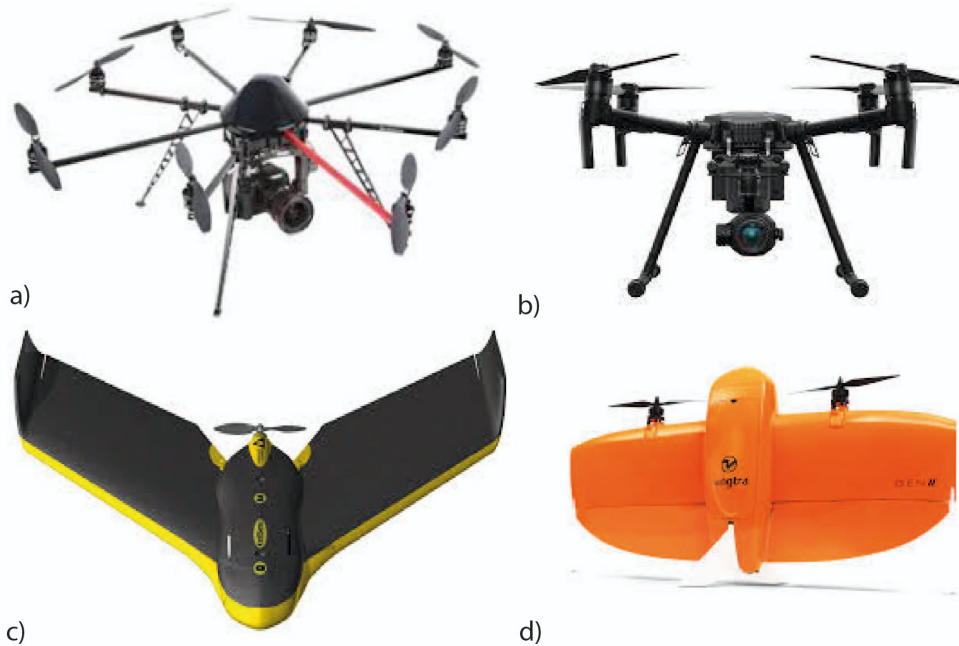
Figure 1. Examples of UAV platforms used in hydrological and environmental studies include rotary-wing UAVs, such as the OktoKopter from MikroKopter (a) and the DJI Matrice 200 Series (b), which offer vertical takeoff and landing, hover capabilities, and low-speed flight for easy control and maneuver. Fixed-wing drones, such as the eBee ultra from senseFly (c) and the hybrid-fixed-wing solution from Wingtra (d), have rigid wings for forward lift, a simple structure, a long flight range, and lower maintenance.

UAVs have critical components such as the frame, navigation system, power system, and payload (Giordano et al., 2016). The frame is made of carbon fiber or plastic and holds all the components, including a Global Navigation System (GNSS) antenna for controlling navigation, flight stabilization, and location data collection. Some drones have a Real-Time Kinematics (RTK) system for real-time corrections (e.g., DJI Phantom 4 RTK, DJI Matrice RTK (SZ DJI Technology Co., Ltd., Shenzhen, China), and accurate positioning data during the flight. Ground Control Points (GCPs) with known coordinates may be needed for geodetic positioning if a drone lacks an onboard navigation system. A geodetic GNSS receiver or Total Station (TS) measures these GCPs (e.g., targets). Although the increasing popularity of UAVs can be attributed to the versatility of rotary-wing multi-copters, fixed-wing platforms are still favored for larger-scale surveys spanning areas such as 1 km^2 owing to their energy efficiency characteristics. Therefore, when planning a study, researchers must carefully consider the limitations of UAV platforms, such as flight duration based on battery capacity and maximum flight distance. In addition, platform selection is also impacted, including user experience, research field, sensor type, required payload, and availability of dedicated software for flight control (Tmušić et al., 2020).

2.4.2 Sensors and Instruments

In environmental science, the following sensors are generally used individually or combined: RGB, MS, HS, TIR, LiDAR sensors, or microwave sensors. This work exclusively describes RGB, MS, and TIR imagery UAV sensing. Table 2 lists different UAV sensors with their advantages, disadvantages, and possible applications.

RGB system

RGB cameras (i.e., digital cameras) capture reflectance in the visible spectrum (0,4 to 0,7 μm) and produce high-quality RGB images (i.e., photographs). These are the most common sensors used in UAVs. These cameras typically have three values for individual RGB pixels and simultaneously capture data from three channels using color filters. UAVs with RGB sensors are easy to operate, relatively inexpensive, and provide high-quality RGB images primarily for dense 3D point cloud creation, orthoimagery (papers II, V, VII), and the development of DEMs (papers I and VI), DSMs (papers III and IV), and Digital Terrain Models (DTMs). The sensor size and focal length are important considerations when choosing a suitable RGB sensor. Larger sensors generally result in higher-quality images, while shorter focal lengths are associated with levels of geometric distortion and require geometric correction (e.g., fisheye lens). The type of shutter utilized is also necessary, with global mechanical shutters offering faster speeds than electronic rolling shutters. Motion blur can be a concern with electronic rolling shutters, which may negatively affect the data quality collected. Flying at low velocities (e.g., 4 ms-1) can minimize this effect, as demonstrated by Vautherin et al. (2016). Similarly, barrel, pincushion, and mustache distortions caused by the camera lens and point of view during shooting are typical in UAV imagery and can affect the object's geometry in the image (Tmušić et al., 2020). *Orthorectification* is a process that can correct these optical distortions and perspective changes resulting from the sensor's viewing angle and position. The rectification plane in aerial photogrammetry is always the XY plane, while in near-object photogrammetry, it can be user-defined. To obtain the third coordinate (i.e., the distance to the object measured perpendicular to the rectification plane), a 3D digital model is necessary to represent the object's geometry. However, with the high point density obtained from SfM algorithms, a reasonably accurate 3D digital model can be obtained (Tmušić et al., 2020).

RGB sensors are used in various applications (Table 2), including stream restorations and sustainability (e.g., paper VI), bathymetry extraction (e.g., paper VII), flood monitoring (Langhammer & Vacková, 2018), surface flow velocity (Kinzel et al., 2019; Legleiter et al., 2018; Legleiter & Kinzel, 2021), water quality (Koparan et al., 2018; Morgan et al., 2020), granulometric studies (paper II and V), and snow research (e.g., papers I and III).

Multispectral (MS) system

MS imaging, the most advanced spectral imaging technique for UAVs, uses a ready-to-use sensor system to deliver high-quality images. These cameras capture reflectance in the visible (Red) to the Near-Infrared (NIR) region (~4,5 μm to ~1,0 μm) and have a narrower bandwidth than RGB sensors. Off-the-shelf MS cameras often operate as multi-cameras that simultaneously trigger all channels (4 to 6). The MS sensors generally capture at-sensor radiance, resulting in RAW images expressed in Digital Numbers (DN). Converting these DN values into absolute surface reflectance values is imperative, as surface and atmospheric interference influence at-sensor radiance (Wang & Myint, 2015). Various techniques exist for this conversion, with the Empirical Line Method (ELM) being the most commonly used during image postprocessing (Aasen & Bolten, 2018). Images of known reflectance surfaces establish an empirical line between image DNs and surface reflectance under survey-specific light conditions (Aasen et al., 2015; Ahmed et al., 2017; Crusiol et al., 2017; Laliberte et al., 2011; Wang & Myint, 2015; Wehrhan et al., 2016). However, the optical device and sensor's spectral response also affects the relationship between DN and surface reflectance value, requiring additional corrections (Kelcey & Lucieer, 2012; Wang & Myint, 2015). I.e., MS sensors can have geometric distortions and spectral/radiometric noise that affect image quality. Comprehensive Field of View (FOV) equipment can introduce radial variation in viewing angle due to solar motion, leading to non-static illumination sources. Clouds can also cause darker spots and variations in DN values, making overlapping stitching images challenging (J. Liu et al., 2016; Stark et al., 2017). Therefore, radiometric correction methods are necessary to overcome challenges with MS UAV imagery. This correction involves correcting the vignetting effect, reflectance, and atmospheric scattering (Honkavaara et al., 2014; Lucas, 1995).

The vignetting effects have three physical causes: natural, optical, and mechanical. They can be reduced through Fourier analysis or a polynomial function (Minařík et al., 2019). The dark current is caused by the thermal stimulation of electrons in solid-state sensors, and it can be reduced by taking an image with the lens covered and subtracting it from all obtained images. Anisotropic properties in

objects, such as the Bidirectional Reflectance Distribution Function (BRDF), can produce various reflectance effects, and their correction involves using a class-specific calibration function (Honkavaara et al., 2014). Atmospheric effects caused by scattering and gaseous absorption depend on flying altitude and study area characteristics, including Rayleigh (when the particles are smaller than the light wavelength), Mie (when the particles are about the size of the light wavelength), and nonselective scattering (when the particles are more significant than the light wavelength).

The atmospheric correction is generally omitted in low-altitude UAV flights. However, in some cases where the quantity of aerosols or haze is high, aerosol sensors could be used, like in Morillas et al. (2013), or a layered scattering physical-based model could be used, like in (Huang et al., 2016). For a more comprehensive understanding of MS photogrammetric processing regarding radiometric corrections, please refer to the works of Minařík et al. (2019) and Minařík & Langhammer (2016).

After all these applied corrections, Vegetation Indices (VI) combining surface reflectance of two or more spectral bands allows calculating advanced VI in the final orthomosaic. MS sensors are rather expensive and heavy, producing coarser pixel resolutions than RGB images. They have mainly used for vegetation monitoring (Assmann et al., 2019; Beyer et al., 2019; Camenen et al., 2016), bathymetry studies (Flener et al., 2013; Lejot et al., 2007), flood monitoring (Brigante et al., 2017), surface and groundwater interaction (Bandini et al., 2017), or water quality monitoring (Koparan et al., 2018). More details are available in Colomina & Molina (2014).

Thermal (TIR) system

Objects on Earth emit radiation in the far infrared spectrum (~3 μm to ~100 μm), and its intensity depends on their surface temperature. Natural objects emit radiation in proportion to blackbody radiation, characterized by their emissivity (ε) value, which varies from 0 to 1 based on their chemical composition and physical structure (Rubio et al., 1997). For example, plant emissivity is around 0.98. Any object above absolute zero emits radiation in the TIR band based on temperature and emissivity.

TIR cameras provide non-invasive visual representations of thermal radiation emitted by objects in the long-wave spectral bands (e.g., ~7.5 μm to ~14 μm). They sense a wide range of temperatures (e.g., -25°C to 135°C) and come with inexpensive, affordable models. Expensive models are more accurate. Low-cost sensors are not radiometrically calibrated and can only provide information on relative temperature differences in raw DN. Two types of TIR imaging sensors are in use: cooled and uncooled. UAV-mounted TIR cameras are usually uncooled because they are small and lightweight (paper IV), but are less thermally sensitive and respond more slowly than cooled sensors. Fisheye effects are observed with FLIR radiometric UAV cameras, and images must be radiometrically calibrated for quantitative assessments (Pajares, 2015). It can be challenging to derive accurate surface temperature measurements, and manufacturers' estimates of temperature precision can be up to ±5°C (or 5% of the reading).

The low accuracy of TIR cameras can be attributed to the uncooled microbolometers used in their Focal Plane Array (FPA). These microbolometers have sensitivity and offset that vary with temperature, and their thermal radiation can interfere with the signal from the object of interest (Olbrycht & Więcek, 2014), resulting in a poor signal-to-noise ratio (Budzier & Gerlach, 2015). Radiometric calibration is necessary to correct these factors. However, the proprietary nature of manufacturer specifications makes it challenging to know how well they account for them (Budzier & Gerlach, 2015; Ribeiro-Gomes et al., 2017; Shaw et al., 2005). Non-Uniformity Correction (NUC) is performed during UAV operations to harmonize the sensor's response signal. However, it may not account for factors such as lens distortion (vignetting) or sudden changes in ambient temperature (Olbrycht & Więcek, 2014). Other factors that affect temperature measurements include object emissivity, humidity, the surrounding temperature, and distance. While low-budget uncooled TIR cameras are more commonly used in UAV applications due to their smaller size and lower weight, methods to minimize their temperature-dependency effects have been described. However, they have not thoroughly discussed this in previous publications (Shaw et al., 2005).

Hence, UAV-based TIR imaging can deliver high-resolution and spatially-resolved surface temperature measurements for environmental applications (Table 2). To ensure accurate calibration, challenges such as spatial non-uniformity, sensor drift, FPA stabilization, and measurement bias must be addressed (Berni et al., 2009; Gerhards et al., 2019; Kelly et al., 2019; Mesas-Carrascosa et al., 2018;

Ribeiro-Gomes et al., 2017; Torres-Sánchez et al., 2013). Thus, pixel values can reliably be converted into surface temperature. Despite its limitations, TIR imagery is widely used in animal monitoring (Briscoe et al., 2014), plant physiology (Still et al., 2019), landscape ecology (Scherrer & Körner, 2011), temperature mapping (Nieto et al., 2022), tile drainage (Tilahun & Seyoum, 2021), evapotranspiration (KUSTAS & NORMAN, 1996), SM (Dai et al., 2022), turbidity plumes (Kolokoussis et al., 2011), groundwater discharge (Lee et al., 2019), and wetland mapping (Jeziorska, 2019). However, it does not provide information on the temperatures of beneath-surface layers (i.e., under the canopy, under a rock, or soil temperatures).

Table 2. Examples of environmental applications, advantages, and disadvantages of different UAV sensors.

Sensors	Environmental applications	Advantages (+)	Disadvantages (-)
RGB sensors	Aerial photogrammetry, DEM, DSM, DTM, change detection, bathymetry, flood monitoring, surface flow velocity, snow, and ice depth	Portable, common, relatively high-quality RGB images for orthoimagery and DSM, easy to integrate with different platforms, low-cost, easy to use	Limited spectral information, lack geometric (e.g. barrel, pincushion, and mustache distortion (Tmušić et al., 2020)) and radiometric calibration
MS sensors	Bathymetry, flood monitoring, surface and groundwater interaction, water quality, snow surface distribution, vegetation mapping, plant physiology, pest-detection	Multiple wavelengths, allow geometric reconstruction and radiometric calibration	Higher cost than RGB, image processing complex compared to RGB, radiometric and atmospheric correction is a must, with limited compatibility with UAVs
TIR sensors	Temperature mapping, tile drainage, evapotranspiration, turbidity plumes, groundwater discharge, thermal inertia, soil water content, plant stress	Sense a wide range of temperatures	Thermally sensitive, vignetting effects, low spatial resolution, radiometric corrections required, sensitive to change in surface roughness and emissivity changes

3. Material and methods

3.1 Background of photogrammetric processing

With the advancement of UAV technology, modern processing approaches have emerged, combining established photogrammetric and computer vision algorithms. These techniques, outlined by Hirschmüller (2008) and Triggs et al. (2000), have led to the development of the SfM and Multi-View Stereo (MVS) processing pipeline (Remondino et al., 2014). SfM-MVS involves capturing the 3D geometry of an object or scene from multiple viewpoints of a moving camera, resulting in high-resolution UAV products with temporal and spatial accuracy, making the process time-efficient, cost-effective, and user-friendly of most photogrammetric products (Fonstad et al., 2013).

3.1.1 RGB photogrammetry

A standard SfM-MVS pipeline for reconstructing overlapping RGB-based UAV imagery consists of three phases: sparse point cloud reconstruction, georeferencing, and dense point cloud generation (Remondino et al., 2011). The process starts with feature-based matching to generate a point cloud of tie points, which includes image observations, internal constraints, and a sparse point cloud. This is achieved through a self-calibrating Bundle Block Adjustment (BBA) without a priori information. The feature-based matching uses collinearity to identify corresponding points in the images based on

epipolar geometry, reconstructing multi-stereo pairs. Subsets of images are incrementally aligned until the complete photogrammetric block is oriented. The Cameras' Interior (IO) and Exterior Orientation (EO) parameters are simultaneously determined through iterations in the least squares sense, minimizing a global reprojection error. This error quantifies the pixel differences between the initially detected corresponding points and those estimated and back-projected into all overlapping images of the photogrammetric block. As a result, space resection and the intersection of every tie point are resolved, and a sparse point cloud with 3D coordinates in an arbitrary coordinate system is generated.

Control information is essential for scaling and orienting the resulting sparse point cloud and photogrammetric block to determine the 3D shape of a surface accurately. This information is typically obtained from surveyed GCPs for indirect georeferencing or from the positions and orientations of the camera exposure stations for direct georeferencing. These control points are weighted observations, external constraints, and tie points (internal constraints) in the least squares BBA. This allows for re-estimating the camera's IO and EO parameters and the 3D coordinates of the sparse point cloud in the desired coordinate system.

Once the epipolar geometry of the photogrammetric block has been established, differences are computed for all pixels using image-matching techniques such as semi-global matching (Gerke et al., 2010; Hirschmüller, 2008). These differences are then used to triangulate the pixels, creating a 3D surface that is smooth and free of abrupt irregularities, achieved through gradient-based and energy-minimization algorithms. This process in the SfM-MVS pipeline results in a dense point cloud with RGB color information, serving as a raw representation of the 3D surface. The georeferenced point cloud, whether sparse or dense, can be exported and interpolated to generate DSMs or DEMs that exclude vegetation or DTMs that represent only the bare ground. These models can be used for various applications, such as generating orthophotos and orthomosaics.

3.1.2 Multispectral photogrammetry

The 3D reconstruction of MS UAV-based imagery follows a similar processing workflow as RGB imagery using commercial software, including tasks such as image alignment, dense point cloud generation, and orthomosaic creation using Agisoft Metashape (Agisoft LLC, St. Petersburg, Russia) or similar software with direct or indirect georeferencing. However, additional processing steps are required due to the unique characteristics of MS sensors, such as radiometric considerations and lower resolution compared to RGB imagery, as mentioned in section 2.4.2. Radiometric processing for MS imagery involves two main phases: radiometric (sensor) corrections and atmospheric corrections. Radiometric corrections aim to restore the normalized DN values to have uniform responses across the image. This can be achieved through relative radiometric calibration, which normalizes DN values concerning a reference, or absolute radiometric calibration, which converts DN values to radiance. These corrections help reduce additive noise and account for changes in incoming radiance from sensors and optics, which may cause vignetting effects and non-uniform quantum efficiency among chip cells (Minařík et al., 2019; Minařík & Langhammer, 2016). Atmospheric correction is performed on top of the radiometric correction results and involves deriving surface radiance or reflectance from the corrected DN values. Newer sensors such as MicaSense, RedEdge, or Parrot Sequoia are equipped with built-in radiometric calibration systems and software like Pix4Dmapper (Pix4D S.A., Lausanne, Switzerland) and Agisoft Metashape can automatically apply these corrections.

3.1.3 Thermal photogrammetry

When generating orthomosaics from TIR images captured by UAVs, a processing workflow similar to RGB and MS imagery with conventional photogrammetric software can be applied. However, it is to consider radiometric corrections specific to TIR imagery in addition to standard processing steps as mentioned above. The output image of a thermal camera may be self-calibrated in radiance, corrected for atmospheric absorption and emission, and converted to surface temperature values for each pixel, depending on the type and age of the camera (Titus et al., 2022). It is important to note that uncooled TIR cameras typically have a lower spatial resolution. Their thermal accuracy can vary based on camera settings, flight planning, weather conditions, corrections, and ortho mosaicing, ranging from ±0.1 to ±5 °C (Kelly et al., 2019). However, to obtain accurate surface temperature measurements, radiometric

correction is necessary. The ELM, which relies on known temperatures of thermal targets on the ground, is commonly used. Four targets, including black (hottest target), white (coolest target), and two intermediate targets (e.g., dry and wet bare soil), are placed on the ground to produce a wide temperature range. These targets are measured continuously during UAV flight using thermo-radiometers and recorded by a data logger (e.g., IR120, Campbell Scientific, ±0.2 °C accuracy when calibrated against a blackbody).

Alternatively, an alternative approach can be applied as used in paper IV. The acquired TIR imagery in paper IV was not radiometrically or atmospherically corrected, even though the FLIR DUO R TIR camera delivers calibrated radiometric temperature measurements for each pixel but with a significant error range thermal accuracy of ±5 °C. A simple linear regression was applied during post-processing to achieve a reliable surface temperature estimation, utilizing sampled ground instrument temperatures and the thermal camera's DN pixel outputs. This approach was chosen to minimize discrepancies and ensure a close alignment with actual surface temperatures. To further enhance accuracy, it is recommended to place ground temperature sensors in areas that exhibit uniformity in slope, composition, and texture, reducing potential errors arising from sensor location within the imagery (Titus et al., 2022). Proper calibration of TIR cameras should ideally be carried out under controlled laboratory conditions that are time-consuming and complex (Budzier & Gerlach, 2015).

3.2 Best practices for UAV-based data collection

Flight planning is critical in photogrammetric projects, impacting data acquisition and processing. Several factors must be carefully considered, including platform specifications (RGB, MS, or TIR imaging), study site extent, terrain sampling distance, payload characteristics, topography, study objectives, weather, and regulations. The workflow developed in this study comprises three phases, incorporating best practices from the literature (e.g., Guan et al., 2022; Tmušić et al., 2020) and the authors' experiences (Figure 2).

The first phase includes pre-mission and on-site pre-flight planning (Figure 2; Phase 1), which involves obeying regulations and obtaining necessary permissions, especially in National Parks (i.e., Šumava NP or Krkonoše NP). Specific requirements such as a pilot license and signed permits are necessary to avoid interfering with flora and fauna, especially during the breeding season. Familiarizing oneself with these rules before conducting a UAV survey is paramount. During phase one, the next step involves defining the project's objectives (Figure 2; Phase 1). For example, this could involve arranging regular grain size analyses to repeatedly chart changes in fluvial dynamics along a river point bar or carrying out SD monitoring to map transformations in the vertical dispersion of snow cover precisely. It is then essential to establish the quality specifications needed for the project, such as the minimum required accuracy in vertical measurements (mean bias) and precision (1σ or RMSE, assuming a normal distribution of data), which can be justified based on the project's requirements. However, this determination demands a preliminary understanding of the features being mapped.

The next step in phase one involves determining the optimal resolution based on the smallest object to be mapped. The Minimum Mappable Unit (MMU) determines the appropriate Ground Sampling Distance (GSD) for mapping objects or features (Singh & Frazier, 2018). When the MMU is small, indicating smaller objects to be mapped, a smaller GSD is needed to capture the desired level of detail, and vice versa. The GSD specifies the size of each pixel in the UAV image captured on the ground, and it is influenced by factors such as camera specifications, flying height, and pixel pitch. Higher flying heights result in a larger GSD, while lower flying heights produce a smaller GSD. A smaller GSD leads to higher image resolution and increased level of detail, while larger GSD results in lower resolution and reduced level of detail. This directly impacts the accuracy and precision of data obtained from the UAV survey, highlighting the significance of MMU and GSD in determining the quality of mapping outcomes.

Once regulations, objectives, quality specifications, and GSD are set, the second phase selects the appropriate sensor (Figure 2; Phase 2). Sensors can be used alone or in combination with other sensors. RGB sensors are suitable for retrieving the snow cover, mapping granulometry, or mapping wetlands. MS and TIR sensors produce lower-resolution images, making them unsuitable for high-resolution topographic mapping. However, the MS camera may be helpful in snow mapping or extracting VIs in

peatland monitoring, providing more spectral information for training a machine or deep learning classification model. At the same time, TIR sensors are beneficial for extracting relative surface temperature only.

The subsequent step in the second phase of the workflow involves selecting the appropriate aircraft to mount the sensor. For our example project, multi-copters were the most suitable option. They can perform vertical takeoff and landing in complex vegetated terrains, fly slowly, and stop to capture high-quality images (reducing motion blur). Moreover, they can hover at low flight heights for close data capture of small objects, and the project's small spatial coverage (e.g., <2 ha) is ideal for low battery capacity. Field checks and proper georeferencing are crucial for accurate and reliable UAV survey results.
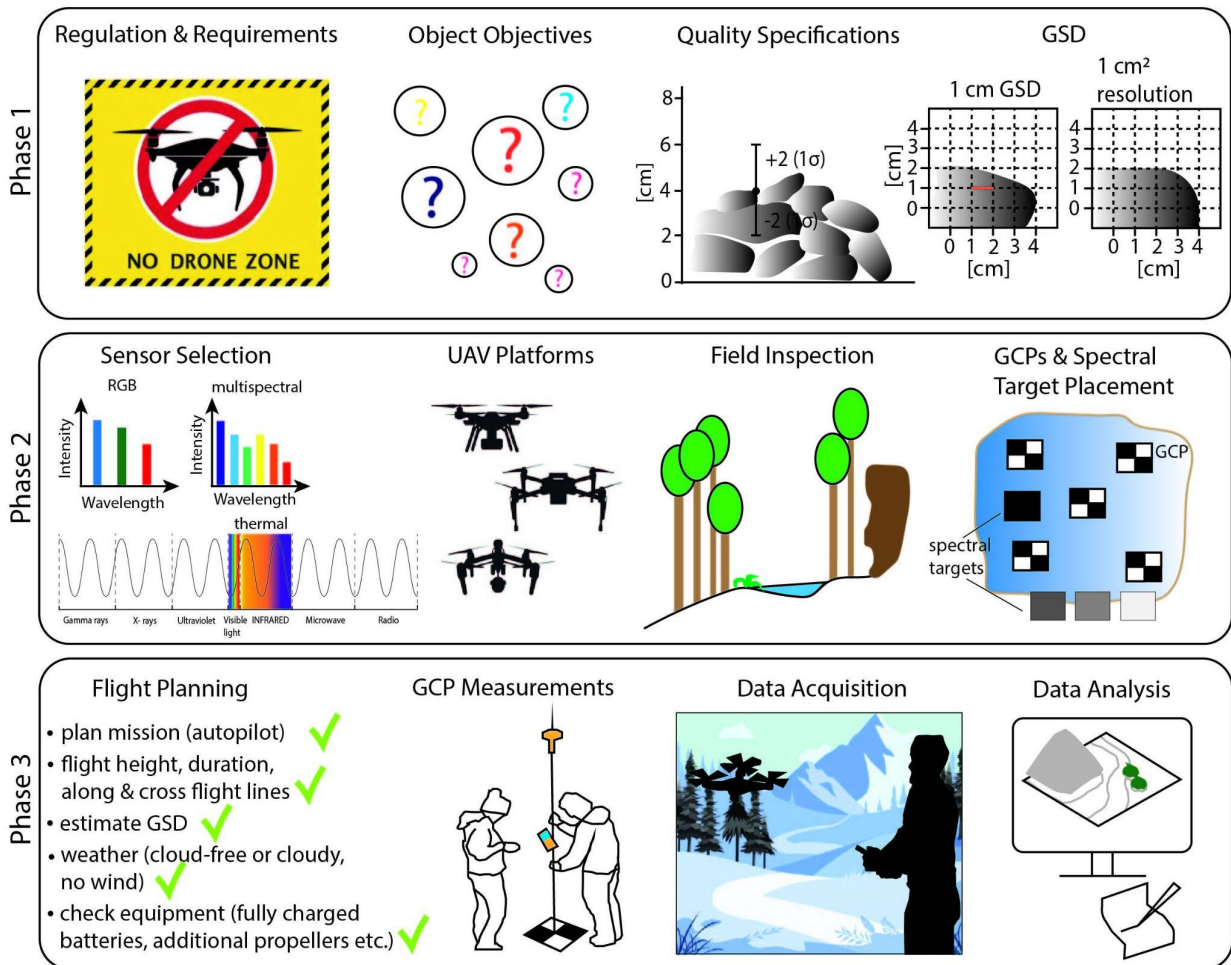
Figure 2. A three-phase workflow was adjusted after Guan et al. (2022) using best practices for conducting RGB, MS, and TIR UAV mapping of environmental subjects.

Evaluating the location for probable obstructions or safety risks, determining suitable zones for taking off and landing, and ensuring adequate, evenly dispersed GCPs (about five GCPs per hectare for planar georeferencing and 10 GCPs per hectare for vertical georeferencing (Manfreda et al., 2019)) are all crucial for precise georeferencing and shape estimation. Likewise, when employing an MS or TIR sensor, it is essential to verify that the spectral targets are correctly positioned for MS surveillance. For reliable detection of GCPs in the thermal domain, composite materials composed of, for instance, styrofoam and black metal have been demonstrated to be effective with thermal data (Perich et al., 2020). Alternatively, black or white polypropylene panels, representing the thermal extremes, may also be utilized and must be visible in the images. Additional GCPs as independent Check Points (CPs) are recommended for unbiased accuracy estimates.

After determining the sensor, aircraft, field reconnaissance, GCP placement, and radiometric calibration targets, the final phase in the workflow is the third phase (Figure 2; Phase 3), which entails planning and executing the UAV surveys. Flight planning can be performed a few days before or on the

day of the mission for precise and efficient data capture. Based on the pilot's skills, autopilot software is recommended (e.g., DJI GS Pro, Litchi, or DroneDeploy). The software adjusts the flight path, flight speed, altitude, image overlaps, and camera settings based on the desired GSD in advance. Manual flights may be required in case of signal loss, saving batteries, or extending the distance. The prevailing terrain and vegetation monitoring methods involve grid or double-grid flight missions tailored to the desired level of overlap (Du & Noguchi, 2017; Pádua et al., 2018; Tahir et al., 2018). However, it is essential to consider the weather conditions, particularly the wind direction, when developing flight patterns, as they can directly affect the quality of data retrieved. For example, the movement of vegetation can significantly impact the accuracy of 3D reconstructions. At the same time, wind speed, illumination, cloudiness, and adverse weather conditions like wind and fog can further undermine the quality of surveys. Both MS and TIR sensors are particularly vulnerable to these factors.

Capturing RGB-based UAV images in RAW format is preferred as it retains more information and allows for enhancements. However, obtaining image data in compressed file formats (e.g., JPEG, PNG) will be sufficient for many applications but will introduce unnecessary noise (Boesch, 2017; Singh & Frazier, 2018). RAW format data have a significantly higher bit-depth, e.g., 12-16 bit vs. 8-bit image information. For example, when setting up a DJI Mavic Pro camera, it is recommended to use an aperture of 2.8, a shutter speed of 1/800, and a minimum ISO of 100. Manual focus is preferred, and weather conditions should be checked frequently. The flight should occur around midday to minimize shadows, and all equipment should be charged, including additional propellers for damage. According to Minařík & Langhammer (2016), MS images are captured in the RAW data format in the initial stage. Then, to make them compatible with commonly used MS image analysis programs, these images are transformed into a single-page TIFF file format using PixelWrench2 (PW2), software provided by Tetracam Inc, like in our case. On the other hand, TIR data is first captured as radiometric JPEGs. For more comprehensive information on MS and TIR image capturing, refer to paper IV. The last steps (Figure 2; Phase 3) include the GCP survey, documenting and storing the data, parameters, and reference data.

3.3 Best practices of UAV data processing

Most SfM-MVS software can be classified into two categories: commercial packages such as Pix4D and Agisoft Metashape, which have standardized workflows and operate as "black boxes" with limited transparency into their internal workings, or open-source software such as VisualSFM and MicMac, which have more complex workflows but allow for more significant internal inspection and understanding by researchers (Tmušić et al., 2020). Utilizing Agisoft Metashape software, the upcoming steps will involve the application of RGB, MS, and TIR photogrammetric techniques. In the case of RGB images, the first step involves uploading the images. When working with RAW images for snow monitoring, more than simply uploading them as the first step may not be recommended. These images often have poor contrast, which can be improved by applying content enhancement or histogram equalization techniques (e.g., Cimoli, 2015) in Adobe Suite. This can result in a wider, more centered histogram, producing higher image quality. To ensure proper alignment with a six-band single multispectral image, each single-page TIFF file must undergo geometric registration before being added to Agisoft software. This process involves performing band-to-band registration followed by band stacking (Guo et al., 2019). Once completed, the MS images can be accurately incorporated into the Agisoft software for further radiometric calibration and analysis (as illustrated in Figure 3, step 1). In Agisoft Metashape, Band 4 is typically designated as the master channel for processing. Similarly, converting TIR images from radiometric JPEG to 16-bit TIFF format is necessary for processing in Agisoft Metashape.

During the second step, removing blurred images is a critical task (Figure 3; step 2). Agisoft Metashape has an automatic image quality assessment feature that identifies images with a value below 0.5 (sometimes 0.7) and recommends their removal from photogrammetric processing (Agisoft LLC, 2021). The value is calculated by assessing the sharpness level of the most focused region in the image, as described by Tmušić et al. (2020). This method effectively determines the appropriate value for RGB and MS images. However, TIR images, which often have lower resolution, typically have values below this threshold. Step 3 involves image alignment using SfM to identify and match standard features, while

step 4 uses BBA to adjust camera parameters and 3D point positions, using a least-squares global optimization approach to reduce image residuals (S. I. Granshaw, 2020; James et al., 2017). Following this procedure, the output is a more dependable, aligned image network that relies solely on the estimated camera positions from the imagery, resulting in a sparse cloud. Step 5 involves quality control assessment of the image network by checking for tie point errors (Cooper et al., 2021; James et al., 2017). The Gradual Selection tool available in Agisoft Metashape facilitates the cleaning process by enabling the selection of points based on three distinct criteria. The *Reprojection error* is one criterion utilized to eliminate points with large residuals, which may be erroneous. When dealing with sharp images, achieving a tie point reprojection error between 0.3 to 0.5 pixels is possible. Another criterion is *Projection accuracy*, which permits the selection of tie points that may be less reliable. The final criterion is the *Reconstruction uncertainty*, which allows for removing points from models with low base-to-height ratios. Tie points at the edges of the project area exhibit a higher degree of reconstruction uncertainty than those in the block center. This is due to reduced lateral overlapping in images covering the edges, as pointed out by Mayer et al. (2018). In step 6, the GCP data should be imported, ensuring consistency with the GNNS data coordinates. Once the GCP data is imported, a manual association of points with their locations is necessary.
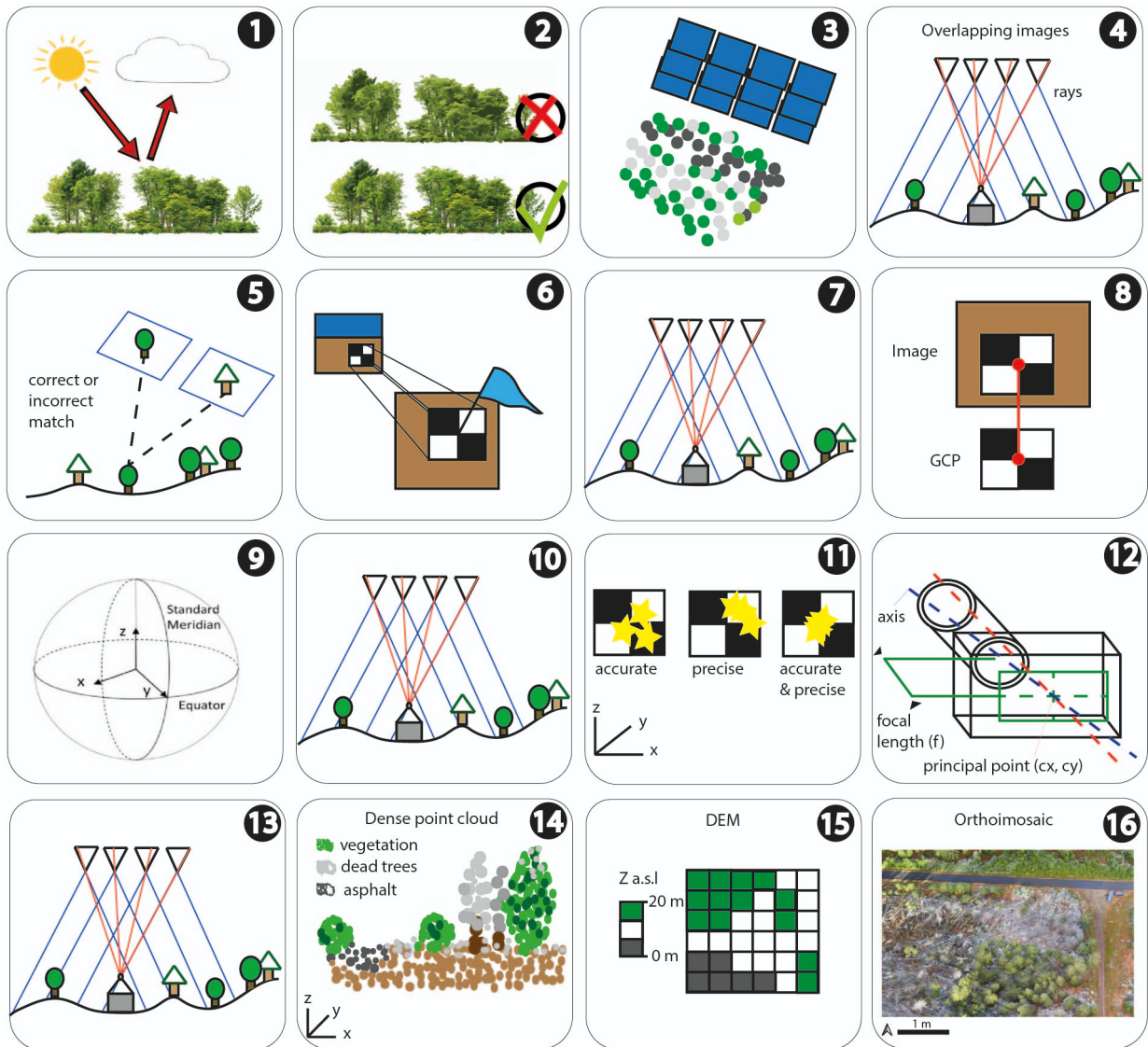
Figure 3. A 16-step workflow was adjusted after Guan et al. (2022) used for processing UAV-based surveys of environmental studies, which includes exceptions and deviations for the MS and TIR photogrammetry.

If using Agisoft Metashape, it is crucial to uncheck all geotagged photos before this step to prevent the production of a distorted DSM resulting from intervening in high-quality GCP data with less

accurate GNNS data (Tmušić et al., 2020). After manually identifying one GCP in two images, the software automatically starts filtering out the remaining images containing the given GCP. Once the software has identified the position of the GCPs, these observations are incorporated into the BBA without being designated as control points and without including their corresponding ground coordinates. This processing technique is commonly referred to as a "free" or "inner constraints" bundle adjustment (S. Granshaw, 1980). It enables assessing the image observations' quality and estimating their measurement precision before they are linked to ground coordinates.

By optimizing camera alignment, georeferencing accuracy can be substantially improved (as shown in Figure 3, step 7) by updating GCPs and camera-estimated coordinates with georeferencing errors. This results in a more precise capture of GCP quality in pixels (as illustrated in Figure 3, step 8), where the RMSE of reprojection is closely associated with estimating planar and vertical positional accuracy, thus leading to a more accurate outcome. Finally, GCPs are linked with their 3D ground coordinates in step 9 for georeferencing, and another BBA is performed using all GCPs as a control in step 10 (Figure 3). To ensure the desired level of accuracy, it is essential to remove GCPs with a high total reprojection error (i.e., more considerable RMSE value) before creating the dense point cloud. It ensures that the image network achieves internal consistency and that high-quality ground control observations are incorporated without significant errors resulting from poorly matched tie points or incorrectly identified GCPs (James et al., 2017). To facilitate this process, a Python script for GCP errors can be exported in step 11, allowing for further analysis of the RMSE values. Moving on to step 12 of the processing workflow, the next step is camera model optimization, which is determined through self-calibration during BBA (Griffiths & Burningham, 2019). One way to assess the error in the GCPs is to randomly select a set of them as CPs and perform another BBA for error evaluation (Figure 3, step 13). This process can be repeated with a different set of randomly selected GCPs as control points until the best possible model is achieved. Accurately determining the magnitude of absolute vertical and horizontal error is paramount in geometric processing (Tmušić et al., 2020). Step 14 generates a dense point cloud with the best-selected CPs, and the resulting point cloud can be classified in Metashape or exported as a LAS file. Steps 15 and 16 involve generating a high-resolution 3D model or orthoimagery (Figure 3). RGB orthomosaics can be exported as GeoTIFF files.

The workflow for MS images remains the same until step 13, but performing reflectance transformation is essential before creating the dense point cloud (Figure 3; step 14). This can be achieved by using values from five reflectance targets based on laboratory values and using the ELM method described by Minařík et al. (2019), such as when using the Tetracam µMCA. So this helps to generate reflectance and normalize signals for different illumination conditions and atmospheric effects. For newer MS sensors, the software typically recognizes calibration and radiometric parameters. However, for more comprehensive details, please refer to paper IV. The workflow for TIR follows the same steps as RGB image processing. From DSM outputs, thermal orthomosaics can be generated to display thermal signatures in DN values ranging, for example, from 0 to 65535, as in our case. Paper IV demonstrates that these DN values can be converted into relative temperatures. MS and TIR orthomosaics can also be exported as GeoTIFF files for further analysis.

3.4 Applied UAVs and camera sensors

In the dissertation, we used a variety of drones with different sensor configurations from RGB through MS to TIR. Some drones had sensors already attached, while others allowed for the attachment of individual sensors as needed. Table 3 summarizes the essential drone and camera specifications utilized in the various papers. It includes information such as drone and camera model, sensor, focal length, flight time, GPS, and the corresponding research paper in which they were utilized. Table 4 provides a separate list of specifications for the MS and TIR sensors. The Tetracam µMCA captures images in the visible and NIR spectrum and the RedEdge component (Table 4). The camera's spectral bands were selected based on previous studies (e.g., Imran et al., 2020; Martínez Prentice et al., 2021; Turpie, 2013) to detect vegetational parameters and monitor changes in peat bog environments. To ensure accurate data, an in-house radiometric calibration was developed for the dissertation (paper IV).

Table 3. Summary of the critical drone and camera specifications used in the papers.

Drone model	Camera model	Sensor	Focal Length	Flight Time	GPS	Paper
DJI Phantom 2 Vision+	Built-in RGB camera	14 MP CMOS, 96° FOV, f/2.8 lens	5 mm	~25 min	GPS	I
DJI Inspire 1 PRO	Zenmuse X5 RGB camera, interchangable cameras	16 MP CMOS, 94° FOV, f/2.8 lens, image size pixel 336 x 256	20 mm (equivalent format to 35 mm)	~18 min	GPS	I, V, VI
MikroKopter Hexacopter	Canon EOS 500 DSLR RGB	18 MP CMOS	20 mm	~15 min	GPS/ GLONASS	II
MikroKopter OctoXL octocopter	Panasonic Lumix DMX-GX7 RGB	16 MP Micro Four Thirds CMOS	20 mm (equivalent format to 35 mm)	~15 min	GPS/ GLONASS	III, V
DJI Mavic Pro	Built-in RGB camera	12.3 MPx camera with 1/2.3" CMOS sensor	28 mm (equivalent format to 35 mm)	~27 min	GPS/ GLONASS	IV
DJI Mavic Pro	Equipped with MAPIR Survey3 Mount holding a FLIR DUO R dual-sensor RGB/Thermal camera	Thermal sensor: Uncooled VOx Microbolometer, thermal measurement accuracy +/-5°C, spectral bands 7.5 to 13.5 μm, image size pixel 160 x 120, FOV 90°	8 mm	~27 min	GPS/ GLONASS	IV
MikroKopter OctoXL octocopter	Tetramcam μMCA (Micro Multispectral Camera Array) Snap 6	5.2 MP CCD sensor, six multispectral filters, image size pixel 1280 x 1024	Micro-MCA cameras use fixed 9.6 mm x-mount lenses	~15 min	GPS/ GLONASS	IV
DJI Matrice 210 RTK V2	Zenmuse X4s RGB camera, interchangable cameras	20 MP CMOS, f/2,8-f/1.1, image size pixel 5472 x 3648	focal length equivalent to 24 mm	~38 min	GPS/ GLONASS/ RTK	V, VII
DJI Mavic 2 Pro	Hasselbad L1D-20c RGB camera	20 MP camera with 1" CMOS sensor, FOV 77°, f/2,2, image size pixel 5472 x 3648	focal length equivalent to 28 mm	~30 min	GPS/ GLONASS	VI, VII
DJI Phantom 4 Pro	Built-in RGB camera	20 MP CMOS with 1" CMOS sensor, FOV 84°, f/2,8, image size pixel 4000×3000	24 mm (equivalent format to 35 mm)	~20 min	GPS/ GLONASS	VII
eBee* (fixed-wing)	Canon S110 RGB camera	12 MP with 1/2.3" CMOS sensor, image size pixel 4000 x 3000, f/8 at all focal length	24 mm - 120 mm	~90 min	GPS/ GLONASS	VII
eBee* (fixed-wing)	Canon S110NIR camera	12.1 MP with 1/1.7" CMOS sensor, acquired false colored images with three channels	24 mm - 120 mm	~90 min	GPS/ GLONASS	VII
DJI Matrice 210 RTK V2	Micasense RedEdge-M multilense MS camera	12 MP CMOS sensor, image pixel size 1280 x 960, five multispectral filters	5.4 mm	~38 min	GPS/ GLONASS	VII

*eBee by senseFly manufacture.

On the other hand, the MicaSense RedEdge-M multi-lens MS camera captures five bands from different lens cones simultaneously - three in the visible spectrum (RGB) and two in the invisible spectrum (RGB, RedEdge, and NIR). Refer to Table 4 for more specifications. The FLIR DUO R dual-sensor RGB/TIR camera captures visible or thermal imaging alone or both simultaneously, with the sensor specifications indicated in Table 4. The combination of the lightweight and compact FLIR DUO R camera, the stable Mavic Pro UAV platform, and the second gimbal allowed us to collect detailed and precise TIR data quickly and relatively efficiently (paper IV).

Table 4. The spectral resolution pertains to the Tetracam μ-MCA Snap 6 camera, MicaSense RedEdge-M, and FLIR DUO R.

Camera	Spectral Bands	Filters	Central Wavelength (nm)	FWHM* (nm)
Tetramcam μMCA	1	Green	550	20
	2	Red	650	20
	3	Red Edge	700	20
	4	Near-Infrared I (NIR)	800	20
	5	Near-Infrared II (NIR)	850	20
	6	Near-Infrared II (NIR)	900	20
MicaSense RedEdge-M	1	Blue	475	20
	2	Green	560	20
	3	Red	668	10
	4	Red Edge	717	10
	5	NIR	840	40
FLIR DUO R	1	Red	660	-
	2	Green	550	-
	3	Blue	470	-
	4	Infrared Radiation (IR)	1000	-

* FWHM: full width at half maximum.

3.5 Study areas

For the dissertation, the study focused on five Areas of Interest (AOI) within the Šumava National Park (Bohemian Forest) located in Southwestern Czechia, three AOI in Prague, Czechia, and two AOI in the southern part of Poland. Two of the areas were chosen for the study of snow cover variations. The first location was an open area with meadow coverage and isolated trees (Figure 4a, b). In contrast, the second location was a forest area dominated by Norway Spruce (*Picea abies* (L.) Karst.) with significant canopy gaps due to bark beetle (*Ips typographus* L.) infestations (Figure 4c, d). The forest area also demonstrated diversity in forest coverage, with one part covered with fallen branches and rotten wood and another covered with still healthy spruce trees but already infected ones in the green attack phase. These two areas with opposing characteristics were used to study the effect of vegetation on snow cover mapping with UAVs, and the data collected was used in papers I and III.
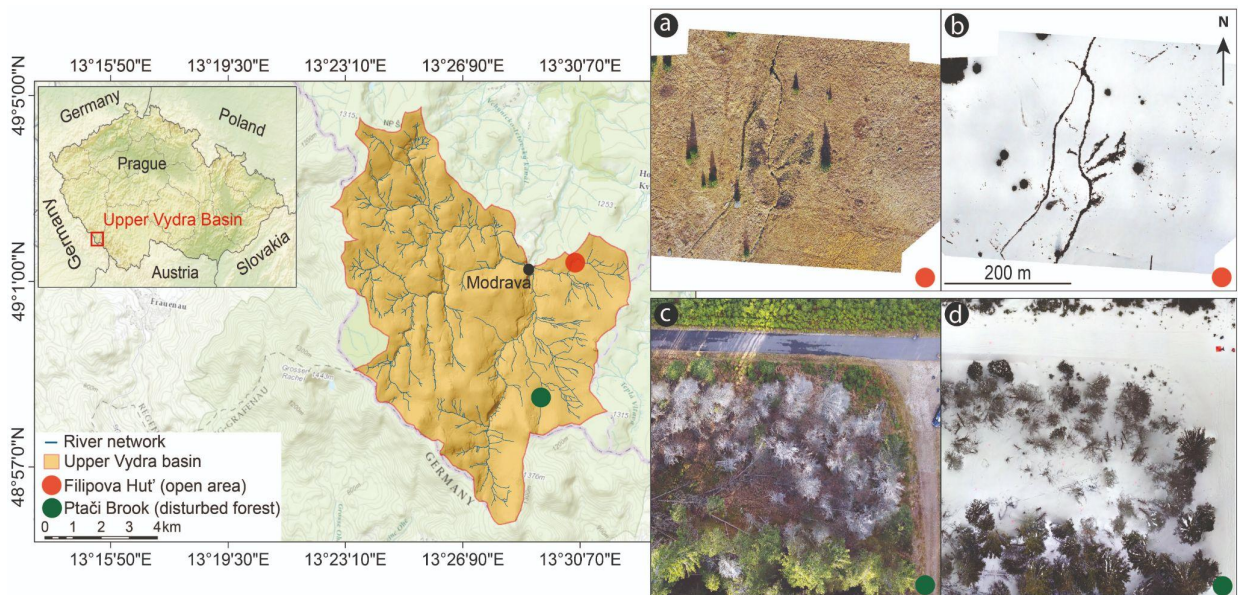
Figure 4. Locality map of the study area southwest of the Czech Republic, near the German border. The Upper Vydra Basin map indicates the locations of the test sites (red and green dots), while the aerial photograph displays: (a) the open area with meadow coverage (snow-free), (b) the same area with snow cover, (c) the forest plot with disturbed forest (snow-free), and (d) the same area with snow cover.

The third locality studied in the dissertation was an experimental area of the Javoří Brook in the Šumava Mts., which represents an unregulated river stream that experienced elevated dynamics of fluvial processes (Figure 5). This area is located in the headwaters of a mid-mountain range and frequently experiences flooding. The area's land use, settlement, and management practices have significantly changed. In the past, the area was surrounded by medieval virgin forests, which were then converted to a forest spruce monoculture for the wood industry after being impacted by bark beetle outbreaks. The study site is a river point bar located at the confluence of the Javoří and Roklanský Brooks, where fluvial processes were started by a flood in June 2013 and heavily accelerated by an early winter flood in December 2015 (Curda et al., 2011). The inner bend point bar exhibits active bank erosion and fluvial accumulations, resulting in consistent changes in PSD (paper V). This makes it an ideal location for studying sediment dynamics within a river system. The experimental site has been utilized in papers II and V of the dissertation.
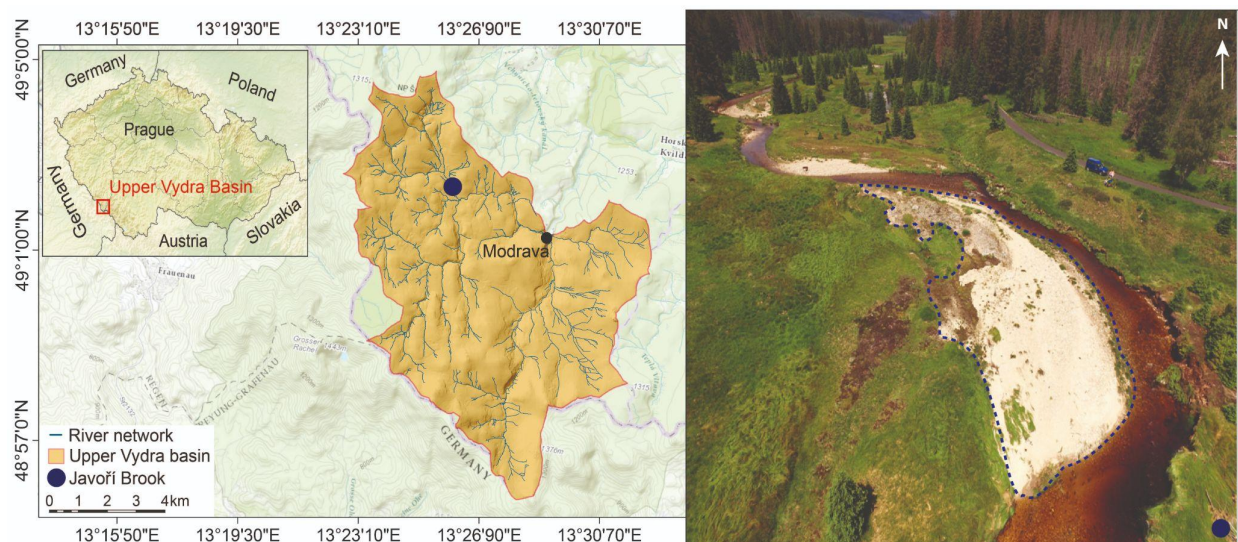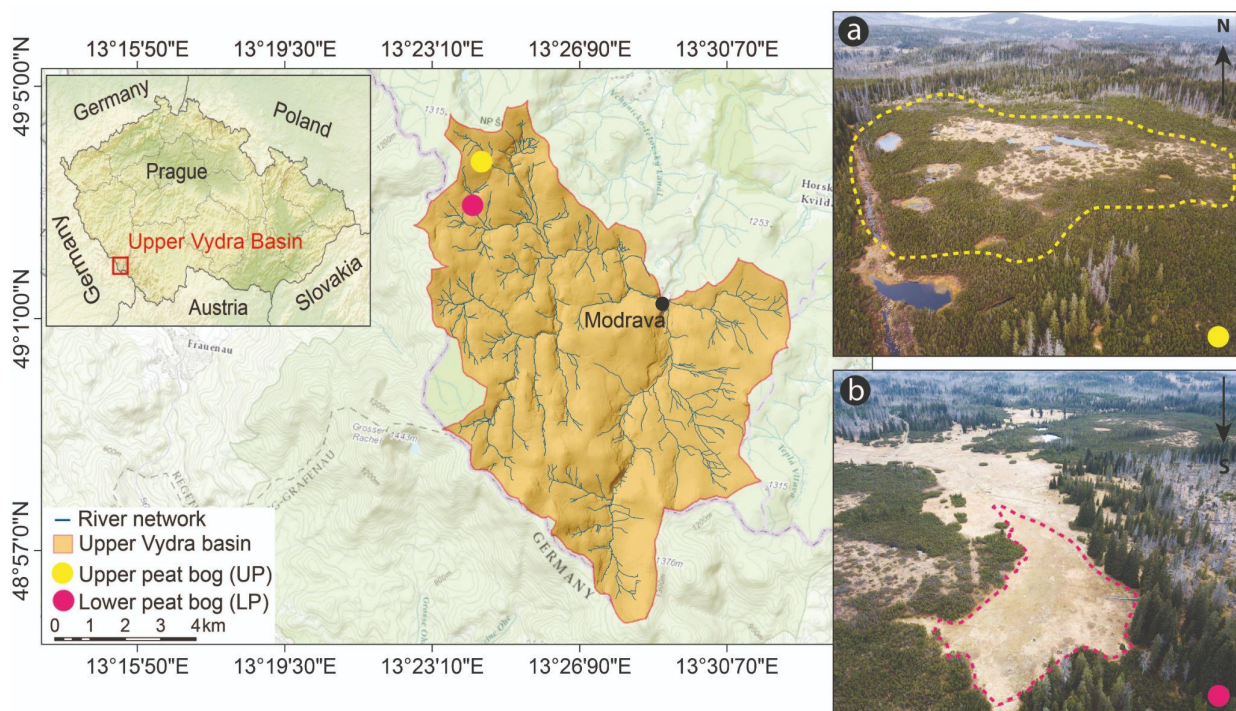

Figure 5. The locality map presents the study area southwest of the Czech Republic near the German border. The Upper Vydra Basin map indicates the test site location (dark blue dot), and an aerial photograph shows the Javoří Brook river point bar.

The Rokytka peat bog in the Šumava Mts. was the fourth and fifth experimental locality studied in the dissertation (paper IV). The peat bog is a large montane-raised ombrotrophic complex covering 250 hectares, and two sites within the complex were chosen for this study. The sites were located along the Rokytka stream and covered an altitude range between 1100 and 1260 m a.s.l. Two opposed test sites were selected to study GWL and SM in this peat bog. The first test site covered an area of approximately 4.5 hectares and consisted of an open treeless site with several pools and a complex system of hummocks and hollows with flat areas in between (Figure 6a). The site was mainly covered by pine *(Pinus mungo Turra)*, blueberry (*Vaccinium myrtillus* L.), and moss vegetation (*Sphagnum* sp.). The second site was a flat zone mainly covered by moss and cotton grass vegetation (*Eriophorum* sp.) (Figure 6b). Both sites contained a well-developed raised ombrogenous peat bog with a Histosol soil type varying from 0.5 m to 6 m depth. Dead spruce trees surround both locality plots, with healthy seedlings at the second site and various dwarf communities. The first site was drained naturally into the local stream, and the vegetation varies based on the water regime. Grass parts without trees are where the groundwater table occurs near the surface, and the soil is primarily saturated with water throughout the year. The second site was most likely affected by one drainage ditch, which drained only a small buffer due to the high hydraulic conductivity of peat. The chosen localities were compared and analyzed to understand the properties and functions of different parts of the peat bog environment from an optical point of view.

Figure 6. The locality map illustrates the study area southwest of the Czech Republic, near the German border. It depicts the Upper Vydra Basin and identifies the locations of the test sites using yellow and pink dots. The accompanying aerial photograph showcases the peat bog's upper (a) and lower sections (b).

In the sixth scenario of the dissertation (paper VI), the Lipanský (LIP; Figure 7a), Rokytka (ROK; Figure 7b), and Hostavický (HOS; Figure 7c) brooks in Prague were selected as study sites due to their varying levels of human impact, ranging from minimal impact in the ROK to heavily impacted in the LIP. The LIP and HOS are comparatively larger streams with a significant amount of human activity, including channelization and discharge of wastewater. Due to this, these streams experience more significant human impact, which can affect the river's morphology and water quality. On the other hand, the ROK is a smaller stream, mainly fed by springs, and has limited human impact. This makes it an ideal site for studying natural river processes and ecosystem dynamics without the influence of anthropogenic factors. The streams are located in valleys with minimal gradients and flat floodplains and historically developed into meandering channels but were gradually straightened and stabilized using concrete profiles due to urban development. This resulted in "new wilderness" zones in the formerly

unmaintained areas. However, after 2000, the City of Prague started a program to restore small streams in the metropolitan area, including the LIP, ROK, and HOS brooks. Restoration works were completed between 2014 and 2018, restoring one to two-kilometer-long stream segments for each brook.
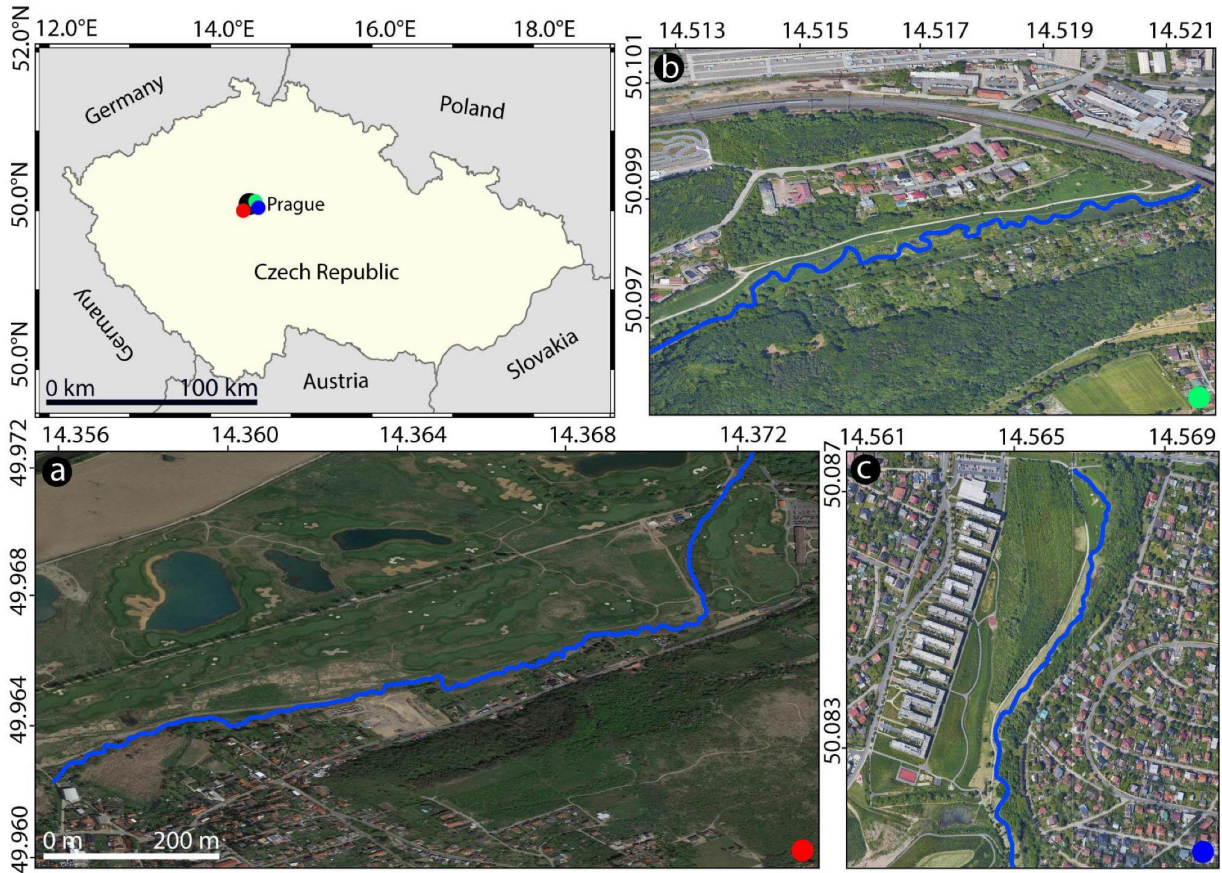
Figure 7. The locality map displays the study area in Prague, Czech Republic, and highlights the locations of the test sites with red, blue, and green dots. The accompanying aerial photographs depict the Lipanský (LIP) brook in (a), Rokytka (ROK) brook in (b), and Hostavický (HOS) brook in (c). The blue markings on the streams indicate the specific sections used to evaluate geometric properties.

In the seventh scenario of the dissertation (paper VII), the study area is in the Izerskie Mountains in southwestern Poland, along the Polish-Czech border (Figure 8). The field experiment was conducted at two sites on Hala Izerska, with Site 1 on a straight segment of the Izera River and Site 2 on a meander northward. The Izera River is a major tributary of the Elbe River. The area has a hilly landscape with minor changes in elevation due to granite weathering. The alluvial channel section represents a natural stream controlled by dynamic fluvial processes, with soft sandy riverbanks and a gravel-sand riverbed. Bank erosion and accumulation of landforms are common due to the lack of training structures and sedimentary material. The channel has asymmetrical banks with erosive undercuts ranging from 0.5 to 1 meter. Different accumulation forms include point bars, mid-channel bars, obstruction bars, and longitudinal bars. The channel width ranges from 4.7 to 17.7 meters, and the average slope of the riverbed is 1.36 ‰. The study section is surrounded by coniferous forest on the right bank and a grassy meadow on the left.
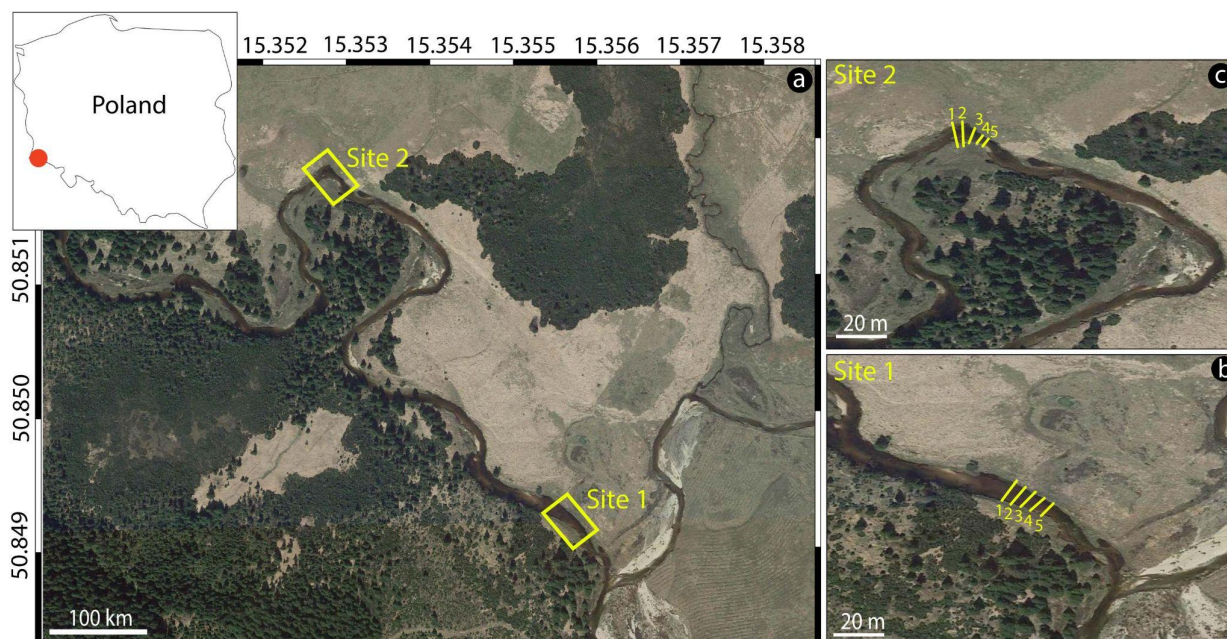
Figure 8. Overview of both studies sites a), Site 1 b), and Site 2 c) location with profile lines.

3.6 Applied methodology

Various methods were utilized for data collection and analysis, with the majority carried out by the author and detailed for each publication in the thesis (see List of publications included in the thesis). These methods included

1. careful planning of UAV campaigns;
2. conducting UAV mapping for snow and forest metrics, peat bog surfaces, and grain size variability;
3. determining their attributes using DEMs, DSMs, and aerial orthoimagery;
4. measuring their surface and subsurface morphology in-situ or using DEMs, DSMs, or aerial orthoimagery;
5. collecting ground samples as a reference and determining their physical properties such as SD, GWL, SM, temperature, or bathymetry;
6. conducting grain size annotation;
7. modeling GWL, SM, and grain size distribution using programming solutions;
8. performing statistical analysis;
9. extensive literature searching aimed at contextualizing the results in broader research or regional contexts; and
10. interpreting and synthesizing the findings.

The UAV imagery was processed using Agisoft Metashape software (formerly PhotoScan; Agisoft LLC, St. Petersburg, Russia), and point cloud filtering was performed using either LAStools software (https://rapidlasso.com/lastools) or CloudCompare software (http://www.cloudcompare.org/). Computation was mainly done using Excel, RStudio, Python, or C++ environments, and further processing of the aerial data was conducted using QGIS (https://qgis.org/en/site/) or ArcGIS10 (Environmental Systems Research Institute) software. All the data and methods used in this study are detailed in the publications themselves (see Supplements) and are not entirely explained here.

4. Overview of published research

This chapter summarizes the results of the dissertation's seven research papers. Four articles were published in the impact journal Remote Sensing (IF2022 = 5.349), one in Sensors (IF2022 = 3.847), and one in peer-reviewed collections *The International Archives of the Photogrammetry, Remote Sensing and Spatial Information Sciences* indexed on Web of Science. Two research papers are being reviewed

in the Journal of Hydroinformatics (IF 3.085) and the International Journal of Applied Earth Observation and Geoinformation (IF 7.672).

4.1 Paper I

Lendzioch, T., Langhammer, J., & Jenicek, M. (2016). TRACKING FOREST AND OPEN AREA EFFECTS ON SNOW ACCUMULATION BY UNMANNED AERIAL VEHICLE PHOTOGRAMMETRY. *International Archives of the Photogrammetry, Remote Sensing & Spatial Information Sciences*, *41*. Vols. XLI-B1 (pp.917-923). Copernicus GmbH https://doi:10.5194/isprsarchives-XLI-B1-917-2016

The study aimed to develop a solution to accurately measure snow cover, volume, and vegetation properties using a combination of SfM and commercial UAV imagery. The study utilized downward-looking UAV RGB-based images to measure winter LAI_{eff} in a spruce forest and to observe SD distributions at two experimental sites, one in an open area and the other in a forested area. The structural arrangement of trees plays a significant role in the observation of snow accumulation and persistence/absence (Baker Jr., 1986; Gleason et al., 2017; Lundquist et al., 2013; Molotch et al., 2009; Varhola et al., 2010), which can affect the accuracy of SD observations due to canopy shading of the ground surface, interception, or reradiation of absorbed energy by trees (Belmonte et al., 2021; Lundquist et al., 2013; Sankey et al., 2017; Zheng et al., 2018). The study compared the retrieved snowpack observations between the open and forested areas and found that the observations of distributed SD values in the open area were in better agreement with manual probing than those with deeper patches of snow in the forest. The study also compared LAI_{eff} estimates derived from ground measurements with UAV LAI data and found that the UAV-based technique showed much closer distribution matches with the Digital Hemispherical Photography (DHP) than the LAI-2200 canopy analyzer (Li-Cor, Lincoln, Nebraska). The study highlights the challenges of using high-resolution centimeter-scale imagery to resolve snow height models with an RMSE at the centimeter level in non-optimal conditions and complex terrain with high vegetation. The study concludes that a quicker-to-apply LAI estimation technique to more accurate sighting ground truth estimates should be found while avoiding significant errors.

4.2 Paper II

Langhammer, J., Lendzioch, T., Miřijovský, J., & Hartvich, F. (2017). UAV-based optical granulometry as tool for detecting changes in structure of flood depositions. *Remote Sensing*, *9*(3), 240. https://doi.org/10.3390/rs9030240

This study utilized optical granulometry and UAV-based photogrammetry to obtain PSDs of selective image tiles from resulting UAV orthoimages along a river point bar and investigate changes in fluvial processes. We tested UAV flight altitudes ranging from 3 to 12 m above ground level to determine the optimal flight altitude for balanced ground resolution, spatial coverage, and image overlaps. We found that an 8 m flight altitude is fair enough for image resolution and photo-sieving, with a moderate volume of image capture and a 70% front and side image overlap. We applied the BASEGRAIN application (Detert & Weitbrecht, 2012) to analyze grain size along point bar transects based on a regular grid and successfully determined eight fractions of grain size percentiles (D_{10}, D_{16}, D_{30}, D_{35}, D_{50}, D_{65}, D_{84}, and D_{90}) for several transects for 2014 and 2016, respectively. Herewith, we demonstrated the potential for greater analytical freedom across multiple study sites and multitemporal analysis of areas experiencing substantial morphological changes. However, the challenge remains in developing a method that can cover larger areas or estimate PSDs over an entire gravel bar rather than analyzing grain size on a single high-resolution aerial orthoimage from a ~1 m^2 patch, as in this and previous segmentation studies.

4.3 Paper III

Lendzioch, T., Langhammer, J., & Jenicek, M. (2019). Estimating snow depth and leaf area index based on UAV digital photogrammetry. *Sensors*, *19*(5), 1027. https://doi.org/10.3390/s19051027

In this study, we conducted a field survey during the snow accumulation and ablation phase of two sites (open area vs. forest area), quasi-extension research of the study in paper I. We continued with indirect LAI_{eff} measurements using UAV-based photogrammetry. We compared the SD measurements obtained through GCPs, a sparse network, with those obtained through a denser network of manual snow probing; there was a much better match. In particular, using a single pixel-based SD extraction from DSMs with fewer samples resulted in better accuracy, with an RMSE of less than 0.10 cm for the open area and less than 0.16 cm for the forested plot. However, when using a 1 m buffer to extract more samples, the uncertainty doubled, with an RMSE of less than 0.17 cm for the open area and less than 0.33 cm for the forested plot. Additionally, we tested two UAV flight altitudes (50 m vs. 65 m) to analyze the difference between indirect winter LAI_{eff} measurements obtained from downward-looking UAV images. We found that the measured LAI_{eff} values depended on the flight altitude, with higher altitudes resulting in lower LAI_{eff} values, possibly due to the narrow camera viewing angle. A lower UAV flight altitude would cover a smaller area but result in more significant variations of scenes and more accurate LAI_{eff} estimates. This study showed that combining UAV-based photogrammetry with field surveys can provide accurate SD and LAI_{eff} measurements in forested areas during the snow accumulation/ablation phase. However, the optimal flight height for achieving the ideal LAI_{eff} estimates using UAV downward-looking images remains challenging.

4.4 Paper IV

Lendzioch, T., Langhammer, J., Vlček, L., & Minařík, R. (2021). Mapping the groundwater level and soil moisture of a montane peat bog using UAV monitoring and machine learning. *Remote Sensing*, *13*(5), 907. https://doi.org/10.3390/rs13050907

This study collected fine-scale spatial data from DSMs, RGB, MS, and TIR UAV imagery to predict in-situ GWL and SM data at two peat bog locations. The study utilized 34 variables as candidate predictors for the CAST ML regression models, which involved microtopographic, vegetational, and temperature drivers. A Forward Feature Selection (FFS) implemented in the CAST package was used to reduce the impact of overfitting caused by correlated variables. The performance test results for each model indicated moderate to solid performance, even though the Lower Part (LP) provided better prediction performance than the Upper Part (UP). The models consistently selected fewer than half of the variables, with temperature and Normalized Difference Vegetation Index (NDVI) being the key variables, followed by variables related to RGB and topomorphometric spectral variables for the UP and topomorphometric and RGB spectral variables for the LP. The study suggests that continued monitoring of the peat bog's topography, morphology, and vegetation will improve our knowledge of the mechanism involved in response to climate change. The approach used in this study can be used to improve the prediction of future responses and sensitivities of peatlands.

4.5 Paper V

Lendzioch, T., Langhammer, J., & Sheshadrivasan, V.K. (2023). Automated Mapping of Particle Size Distribution from UAV - imagery using the CNN-based GRAINet Model. Journal of Hydroinformatics. IF 3.085 (under review)

The study builds upon the findings of a previous study (paper II) by introducing a new automated data-driven approach called GRAINet for estimating PSD characteristics on entire gravel bars using georeferenced UAV images. The GRAINet methodology utilizes a CNN architecture to directly predict PSD characteristics from image textural features, including mean diameter (*dm*). The method is tested

on eight UAV datasets from a point bar of a montane stream in the Javoří Brook Šumava National Park in Czechia. The model is trained on diverse annotated training sets and evaluated for prediction accuracies. The GRAINet algorithm demonstrates high to moderate accuracies in predicting mean *dm* but tends to underestimate most models. Statistical analyses on image tile properties reveal that saturation and contrast have a more significant influence than image tile sharpness or orthoimage. The GRAINet approach provides an efficient and automated means of estimating PSD, enabling prompt decision-making based on high-resolution grain size maps, even without direct object counts or probes.

4.6 Paper VI

Langhammer, J., Lendzioch, T., & Šolc, J. (2023). Use of UAV Monitoring to Identify Factors Limiting the Sustainability of Stream Restoration Projects. *Hydrology*, *10*(2), 48. https://doi.org/10.3390/hydrology10020048

The study used UAV monitoring to assess the sustainability of stream restoration projects in Prague, Czech Republic. Based on six years of monitoring, we analyzed restoration's quantitative and qualitative aspects, such as the restoration effect, fluvial processes, hydrological connectivity, and riparian vegetation. The photogrammetric reconstruction of the riverscape models provided a basis for visual assessment. Using existing classification schemes and data, we were able to detect critical features accurately. The results showed significant discrepancies in channel geometry between the planned and realized restorations and issues in qualitative aspects, such as water overuse, eutrophication, and inefficient riparian shading, which limit restoration quality. The restored channels were less complex and featured a simpler geometry than planned, which negatively affected the positive effect of the projects and limited their sustainability. UAV monitoring also revealed qualitative shortcomings in the restorations, including stream segments featuring instability and disruptions of hydrological connectivity. Using UAV monitoring with existing assessment methods can facilitate better information on stream restoration effectiveness and sustainability.

4.7 Paper VII

Witek, M., Walusiak, G., Halicki, M., Remisz, J., Borowicz, D., Parzóch, K., Kasprzak, Ł., Langhammer, J., Gallay, M., Miřijovský, J., Šašak, J., Kaňuk, J., Lendzioch, T., Minařík, R., Popelka, S., Niedzielski, T., 2023. Reconstructing bed topography of a shallow river from close-range aerial imagery: multi-drone experimental campaign in the Izera river (SW Poland/N Czechia). International Journal of Applied Earth Observation and Geoinformation. IF 7.672 (under review)

The study's objective was to use the SfM algorithm to reconstruct the bathymetry of a shallow Izera river in SW Poland/N Czechia. We conducted a multi-drone experimental campaign using one fixed-wing drone (eBee by SenseFly) and three multi-rotors (DJI Matrice 210-RTK V2, DJI Mavic 2 Pro, DJI Phantom 4 Pro) to evaluate the robustness of the approach by exploring its repeatability and reproducibility. The riverbed topography was reconstructed 48 times using the SfM algorithm and corrected for refraction. The reference elevations of the riverbed were obtained using leveling, while a TLS determined water surface elevations. We found that the RMSE of the reconstructions of bottom river topography varied between 2.6 cm and 109.3 cm, with a median of 17.5 cm, and was mainly underestimated. The repeatability test for all platforms had an RMSE smaller than 10 cm in 57% of the cases and up to 76% for only multi-rotors. The reproducibility test had an RMSE smaller than 10 cm in 47% of the cases and up to 60% for only multi-rotors. Hence, we concluded that the approach is robust regarding its repeatability and reproducibility, mainly when multi-rotors are utilized. However, the effectiveness of the bottom reconstruction depends on the channel morphology and decreases explicitly in the vicinity of the river banks.

5. Discussion

The thesis provides insights into using UAV RS technology for studying cryosphere science, geomorphology, river sustainability, river bathymetry, and peatland dynamics in mid-latitude montane

regions, specifically, the Šumava region of Czechia, Prague, and southern Poland. These unique regions with complex topography and hydrology are ideal for understanding natural ecosystems and developing management strategies. Integrating UAV-based data with ground-based measurements and models is emphasized to improve prediction accuracy. Findings have implications for future environmental research and resource management.

5.1 SD and the indirect LAI retrieval from UAV images

The study (paper I) shows that the RGB camera in the visible spectrum can capture SD distributions in open and forested regions and the impact of vegetation on SD variability. Previous work supports these SD analysis results, even without additional NIR input (e.g., Avanzi et al., 2017, 2018a; Bühler et al., 2016; Nolan et al., 2015). Although photogrammetry on snow-covered terrain was previously deemed infeasible due to low contrast, recent studies have overcome these limitations. However, creating precise and accurate SfM DEMs/DSMs of homogeneous snow cover can be challenging due to the difficulty that SfM software faces when attempting to determine matching points using an RGB sensor on a smooth snow surface. In order to tackle this challenge, it is crucial to consider several factors that can affect the precision and accuracy of the resultant snow-free and snow-covered models. In particular, these factors include weather conditions, flying height, distance to GCPs, image overlap, and field site conditions such as vegetation. Among these factors, illumination and cloud cover can significantly impact image quality, potentially leading to incomplete or inaccurate 3D reconstructions. Conversely, the combination of low temperature and wind can limit flight duration and pose a safety risk to those involved in the survey. In addition to wind speed and direction, air humidity plays a significant role in image quality. Higher humidity levels contribute to greater light dispersion, making creating accurate 3D snow cover models more difficult.

Reasonable vertical accuracies were achieved in the SfM models in paper I, despite the cloudy weather conditions during the surveys. The snow-covered DEMs exhibited particularly good accuracies. It is noteworthy that Revuelto et al. (2021) found that a clear sky at noon would lead to more homogeneous illumination and greater coverage in the SD map. However, the lower accuracies of the bare ground DEMs were primarily due to the open area SfM survey conducted over a more uniform vegetational surface comprising single trees, high thick grass, and hummocks in between. Dense vegetation types can obscure the line-of-sight of the actual ground level and introduce additional bias in vertical model accuracies (Goetz et al., 2018; James et al., 2017). As reported in other studies (Adams et al., 2018b; Bühler et al., 2016; Nolan et al., 2015), the same issue can arise with dead tree stumps lying on the ground (e.g., Stevenson et al., 2015; Wierzbicki, 2017).

In paper III, we showed that the precision of bare-ground DSMs improved even under different weather conditions. However, partly clear skies were not ideal due to fleeting shadows on the ground, especially in the forest, which can affect the flight mission configuration regarding data gaps. To overcome this issue, we recommend using a k-means clustering algorithm after Jain (2010) removes light and hard shadows on snow-covered point clouds and improves the precision of the snow-on or snow-off DSMs. To assess the accuracy of our results, we compared the vertical SD accuracies obtained from our study with manual probing using either a pixel-based approach or denser snow probing networks. We found that our results were as good and aligned with the results of other studies (e.g., Avanzi et al., 2017, 2018b; Bühler et al., 2016; Cimoli et al., 2017; De Michele et al., 2016; Harder et al., 2016; Vander Jagt et al., 2015). However, it is crucial to note that the accuracy of snow probing is also influenced by local snowpack characteristics and the underlying ground, such as vegetation and microtopography, which can result in estimation errors at the centimeter to decimeter level (Adams et al., 2018a; Bühler et al., 2016; Fernandes et al., 2018; Harder et al., 2016). In paper III, we improved the accuracy of our SD measurements by accounting for the effect of vegetation compression by the snow, which was observed as the most significant negative value showing an underestimation of SD for UAVs, especially in paper I. However, confounding effects due to vegetation remain a common phenomenon in the snow community, as observed in other studies (i.e., Bühler et al., 2016; Eberhard et al., 2021).

To our knowledge, low-cost downward-looking UAV-based images have not yet been applied to investigate the indirect winter LAI_{eff}, which considered the clumping effect of leaves in a canopy causing LAI measurements to overestimate or underestimate the amount of leaf area. The direct methods usually

obtain vegetation LAI by manually sampling leaves and measuring their total area using a leaf area meter, which is destructive, time-consuming, and labor-intensive (Yan et al., 2012). Alternative, less destructive, and well-established instruments for indirect LAI measurements are, e.g., the LAI-2200 plant canopy analyzer (Li-Cor, Lincoln, Nebraska) or DHP, two of the most common devices. Otherwise, downward-looking UAV images can be used. The basic technique is the same as used in DHP analysis (Chianucci & Cutini, 2012; Jonckheere et al., 2004; Miller, 1967); the difference is that the background is the snow-covered terrain instead of the sky.

Paper I provides some of the earlier results of the simultaneous UAV mapping of SD and the indirect winter LAI_{eff}. *Randomization* is a widely used statistical method often employed in experimental designs to reduce the effects of bias and confounding variables (Smith, 1998). In the context of UAV-based LAI estimation, randomization can help ensure the representativeness and generalizability of the data distributions and minimize the potential impact of systematic errors in allocation. In paper I, we used randomization to assign and rank the extracted winter LAI_{eff} data (i.e., LAI-2200, DHP, and UAV-based LAI_{eff}) randomly from the highest to the lowest values to assess the quality of the random selection rule. The results showed relatively high relationships between the different LAI methods using this simple statistical method, indicating that the randomization effectively reduced bias and confounding variables.

However, we used a local control experiment in paper III, where data was matched based on specific variables assigned randomly to a group at a specific location to ensure that the data at the exact location is as similar as possible regarding the character being controlled. For instance, plot number one corresponded to the first extracted values from each method; plot number two corresponded to the second extracted values from each method, etc., and were then compared. This method decreases the experimental error and increases the efficiency of the experimental design (Yu & Kumbier, 2017). Usually, the detected forest area should be by ground-based techniques, and drone LAI measurements are about the same, but the drone LAI measurements were somewhat underestimated (paper III). One potential source of bias is the presence of intercepted snow at the tree canopy, which can cause an underestimation of LAI values. This is because intercepted snow can block the view of leaves, making it challenging to measure leaf area accurately. However, once the snow ablates and the tree canopies become snow-free, the correspondence between drone LAI measurements and other techniques can improve. Nonetheless, the non-completely snow-covered forest floor (e.g., the presence of snow uncovered lying wood on the ground and shadows) also affects the accuracy of LAI measurements because the forest floor should be wholly snow-covered and act as a light background for the hemispherical analysis of the images. Therefore, it is essential to consider the characteristics of the forest floor when interpreting LAI measurements obtained using drone technology.

Another aspect is the flight height of the UAV. As the flight increases, the image's resolution decreases, making it more challenging to measure the leaf area accurately. Additionally, the flight height can also affect the angle of incidence of the light captured by the camera; with increasing flight height, the angle of incidence becomes more oblique, affecting the amount of light reflected by the presence of needles and branches. This can cause shadows and other artifacts, making measuring the LAI precisely from a downward-looking view more challenging. It is recommended to use a lower flight height to capture images with higher resolution and a more direct angle of incidence to make accurate LAI measurements in spruce forests. The optimal flight height depends on the specific characteristics of the forest and the resolution and accuracy requirements of the study. Paper III presents this pattern, where the LAI values decrease with higher flight height. At higher altitudes, the camera sees a larger area, which means that the LAI values captured are more likely to be averaged across a larger area. This may result in less variation in the LAI values captured, as the camera is capturing a broader, more representative sample of the canopy. In contrast, the camera sees a smaller area at lower altitudes, which means a higher variation in the captured scenes. This is because the camera is more likely to capture a smaller, more localized area with a different LAI value than the surrounding area.

Although LAI is not directly related to SD, it serves as an indicator or proxy to evaluate the accuracy of SD measurements obtained by the UAV. High LAI values suggest less snow accumulation and lower SD readings in these areas, whereas low LAI values suggest more snow accumulation and higher SD measurements. Hence, LAI and snow accumulation have an inverse relationship (Jost et al., 2012). Therefore, using LAI as a proxy can help to improve the accuracy of SD measurements obtained by

UAVs, particularly in areas where vegetation density varies significantly. However, the relationship between LAI and snowmelt is complex and depends on various factors, including temperature, precipitation, wind, sun angle, canopy snow-holding capacity, vegetation cover, and soil moisture. For instance, some intercepted snow may sluff off the canopy, particularly in dense forest areas, and contribute to snow accumulation on the ground. Dense canopies absorb and convert more solar radiation into heat, reducing solar radiation reaching the ground and slowing down melting. Sparse canopies allow more solar radiation to reach the ground, increasing surface heat and accelerating snow melting. We found lower relationships between SD and LAI during snow ablation in paper III. Some outliers' tendencies showed a slight correlation between higher LAI values and SD. One assumption is that some of the intercepted snow sluffed off the canopy, mainly intercepted snow of the denser forest areas, and was added to beneath-forest accumulation (Lundquist et al., 2013). Alternatively, as stated above, a denser canopy reduces the amount of solar radiation that reaches the ground and slows the melting process. Consequently, in papers I and III, we obtained low-cost RGB imagery using UAVs, and all the methods used in the studies could make relatively accurate predictions.

5.2 UAV optical grain size detection

The studies (papers II and V) used optical UAV-based imagery to develop and test classification procedures for determining grain size percentiles and characteristics of fluvial deposits along a river point bar over time. The earlier study (paper II) used a segmentation-based approach (Detert & Weitbrecht, 2012), while the more recent study (paper V) used a CNN framework (Lang et al., 2021), which enables the remote measurement of grain size from georeferenced images. Segmentation-based approaches involve dividing an image into regions based on specific criteria and then analyzing each region separately. In the case of the study in paper II, the river point bar image was segmented based on color and texture to separate different material types, including sand, gravel, and larger rocks only at the surface. The segmented regions were then classified into different grain size categories.

In contrast, the DL approach used in paper V is a more automated indirect method of PSD determination based on texture and neural networks that can analyze granulometry across entire orthomosaic images. The DL algorithm first segments the image into small patches and then classifies each patch as clasts or background material. The clasts are further segmented and classified based on size, shape, and texture. This method requires less manual intervention and can analyze larger areas more efficiently than the segmentation-based approach used in paper II. However, like any DL algorithm, it requires a substantial amount of training data (lots of labeled images) to be effective, and the quality of the training data can affect the accuracy of the results. While both approaches have strengths and weaknesses, the segmentation-based approach used in paper II might provide more accurate results but is more time-consuming and subjective (Chardon et al., 2022) and can only be used on individual image tiles. Using the default options for each step is recommended to decrease the processing time of each image tile (Chardon et al., 2022).

In contrast, the DL approach is more efficient and automated for analyzing granulometry across larger areas. However, it is a relatively new method, and more research is needed to fully understand its potential and limitations. The accuracy of the result hinges mainly on the quality of the images and the orthoimage itself, which includes factors such as sharpness, contrast, and color accuracy. While image resolution may have a minor influence, the dataset used to train the CNN can significantly impact the model's ability to generalize to new data (paper V). Hence, obtaining high-quality images with minimal distortion and precise identification of objects is essential for accurate analysis using segmentation-based and DL approaches. Low-altitude overflights in stable weather conditions are recommended to capture high-resolution sediment accumulation, as papers II and V suggested. However, simplifying clast schematization in 2D space is a limitation of these methods. Accurate identification of objects and their shapes is also influenced by other factors, such as image compression, uniform lighting conditions (one of the most crucial factors), and the absence of shadows. Therefore, carefully considering and selecting imaging equipment and image processing techniques is necessary to ensure the best possible results.

5.3 Limitations of the sustainability of stream restoration projects

The study (paper VI) highlights the potential of using high-resolution optical imaging from UAVs and photogrammetric reconstruction techniques for assessing various aspects of fluvial geomorphology and stream restoration. The high-resolution imagery obtained from UAVs equipped with RGB cameras can be used for detailed topographic reconstruction using the SfM algorithm. This allows for rapid field mapping and objective determination of discrepancies in geometric properties of the riparian zone at a centimeter-level resolution. However, optical sensing is limited by the direct visibility of scenes and riparian vegetation, and overhang canopy can obstruct the mapping of channel properties in natural landscapes. Multiple views of an object from different angles can partially solve this problem, and scheduling imaging campaigns during the vegetation season can help bypass extensive obstruction by a deciduous canopy (paper VI). Alternatively, one way to address this issue is using NIR or HS sensors, which offer advantages. NIR sensors can penetrate vegetation to some extent (depending on the thickness and density of the vegetation, type, and sensitivity of the sensor being used), enabling the mapping of submerged aquatic vegetation. In contrast, HS sensors can provide more detailed information on vegetation composition and other materials on the riverbanks and channel. Nevertheless, these sensors are more expensive and require more processing than standard RGB cameras despite their benefits, particularly HS sensors.

Based only on optical UAV monitoring, paper VI found that the restored vegetation and planned habitat diversification did not fully recover due to insufficient or improper maintenance. This led to potential ecological and hydromorphological quality declines. Therefore, it is essential to include post-project monitoring and evaluation in the design and implementation of restoration projects to ensure their effectiveness and long-term sustainability. Furthermore, UAV monitoring enabled the identification of issues related to vegetation restoration. During the restoration projects aimed to restore the vegetation along the streams, the monitoring revealed that the restored vegetation was only sometimes thriving.

In some cases, the vegetation did not grow at all, while in other cases, the vegetation growth was dominated by invasive species. Additionally, vegetation restoration often fails to restore the natural structure and diversity of the riparian zone. It is clear that while the restoration projects have improved the streams' geomorphological properties, issues still need to be addressed. The need for more complexity in the restored channels compared to the approved plans and issues in flow continuity and hydrological connectivity demonstrates the need for better planning and monitoring of restoration projects. The specific issues identified in each catchment also highlight the importance of considering local conditions and potential impacts on the ecosystem when designing and implementing restoration projects. The study found that stream restoration projects' quantitative and qualitative aspects must be assessed to ensure their effectiveness and sustainability. While traditional field surveys are essential, UAV monitoring using RGB sensors has the potential to provide reliable spatial information on critical parameters such as stream geometry, flow continuity, water quality, and riparian shading. Although UAV monitoring cannot replace field surveys for all ecohydrological parameters, it can be a valuable tool for routine monitoring of restoration projects and providing information compatible with standard monitoring schemes.

5.4 Obtaining river bathymetry

The study (paper VII) found that the UAV-SfM approach for reconstructing river bathymetry is a robust and repeatable method for assessing bottom river topography, with RMSE values ranging from 3.8 to 109.3 cm on site 1 and 2.6 cm to 32.1 cm on site 2. These results are consistent with other studies assessing the accuracy of remote reconstruction of submerged landforms in different rivers and coastal areas (e.g., Figueiredo & Rockwell, 2022; Li et al., 2019). However, the limitations of the method depend on factors such as the types of UAVs and sensors used, river channel morphology, and the transparency of the water. Clear water conditions are ideal for reconstructing riverbeds, while water surface roughness, turbulence, and suspended sediment can constrain the accuracy of the reconstruction. Disturbances on the water's surface can also cause ambiguity in the location and shape of objects. Thus, while the UAV-SfM approach is a reliable tool for assessing river bathymetry, it is essential to consider

these limitations when interpreting the results. The accuracy of obtaining an accurate bathymetric model is affected by various factors, with the refraction effect at the air-water interface being one of the most complex. To accurately reconstruct the river bed, the refractive index must be considered. The refractive index used in this paper was 1.34, which is suitable for clear water but may not be appropriate for all river channels.

Additionally, uneven water surfaces may cause the refractive index to vary between images or within a single image, further affecting the accuracy of the reconstruction. In most cases, the reconstructed river bed elevation was underestimated, which could be due to the refractive index needing to be set higher. On the other hand, in some cases, the elevation was overestimated. Therefore, accurate bathymetric modeling requires careful consideration of various factors, including the local conditions and the refractive index. Meteorological conditions are essential in UAV data acquisition and subsequent topography reconstructions. The weather conditions during the flights must be similar to ensure these factors do not affect the results. It is also crucial to consider how the water's surface is lit, as the sun's glint and reflection can make it difficult or impossible for the light to reach the channel bottom. Reflections and overexposure were detected on only a few images, and they had no impact on SfM-based spatial data and, thus, on reconstructions of bottom river topography. However, the results can vary more due to the specificity of sites and the location of profiles delineated within sites rather than due to meteorological or lighting factors. Studies have shown that the UAV-SfM approach is robust to variable lighting conditions, as consistent results of bottom reconstructions have been achieved under changeable lighting conditions. The effectiveness of river bottom reconstruction using UAVs depends on several factors, including river channel morphology and the accuracy of determining the position and elevation of the water surface. The reconstruction accuracy decreases near river banks, especially in the coastal zone, due to incised, steep banks covering the bottom and shadows from riparian vegetation. The accuracy of the reconstruction also depends on the depth of the river, with deeper water bodies requiring higher accuracy in determining the position and elevation of the water surface. Using highly precise TLS for determining water table elevation reduces errors due to inaccurate water table determination. The accuracy of the bottom reconstruction is compared to reference measurements of submerged topography produced by leveling, which may be affected by difficulties in reaching the water-land interface and the impossibility of proper location of the initial benchmarks. This study confirmed the effectiveness of the method of river bottom reconstruction using UAVs, and the high efficiency of this method was confirmed, especially for multirotor. Despite the not completely satisfactory results of the bottom reconstruction, the repeatability and reproducibility of the method were proved.

5.5 Estimating GWL and SM based on multiple UAV datasets

Paper IV presents a study that combines UAV imagery and ML to extract microclimatic variables that might control GWL and SM in an ombrotrophic peat bog environment. We used a multi-step process that involved using UAVs equipped with RGB, MS, and TIR sensors to capture high-resolution images of the surface and subsurface features over two peat bog sites. We then used a derived suite of variables from DSMs, RGB, MS, and TIR datasets to predict the connection probability of GWL and SM. The primary goal was to understand if the extracted microclimatic variables can improve the knowledge and understanding of the patterns of GWL and SM in peatlands. While elevation models based on remotely sensed data have been used in peatland research in the past, ranging from delineating and identifying wetlands and peatlands within a broader ecological landscape (e.g., Chasmer et al., 2020; Hird et al., 2017) to mapping water-table depth (Rahman et al., 2017) and microtopography within individual peatland (Lovitt et al., 2018), this study is the first demonstration of using multiple UAV-based datasets as an exploratory tool for understanding the natural patterns of GWL and SM in peatlands. We used the CAST algorithm to model the relationship between morphometric, topographic, vegetational, and temperature-related variables and GWL and SM based on the method by Meyer et al. (2018). We also used the FFS method with a target-oriented Leave-Location-Out (LLO) Cross-Validation (CV) strategy to select the most critical variables. We estimated the Area of Applicability (AOA) to evaluate the transferability of the models. Using the CAST prediction method and target-oriented LLO CV validation, the modeling of GWL and SM may have resulted in less accurate prediction maps with high

R^2, low RMSEs, and low MAEs having better-achieved results with GWL and SM predictions at the LP than at the UP (Figure 9).
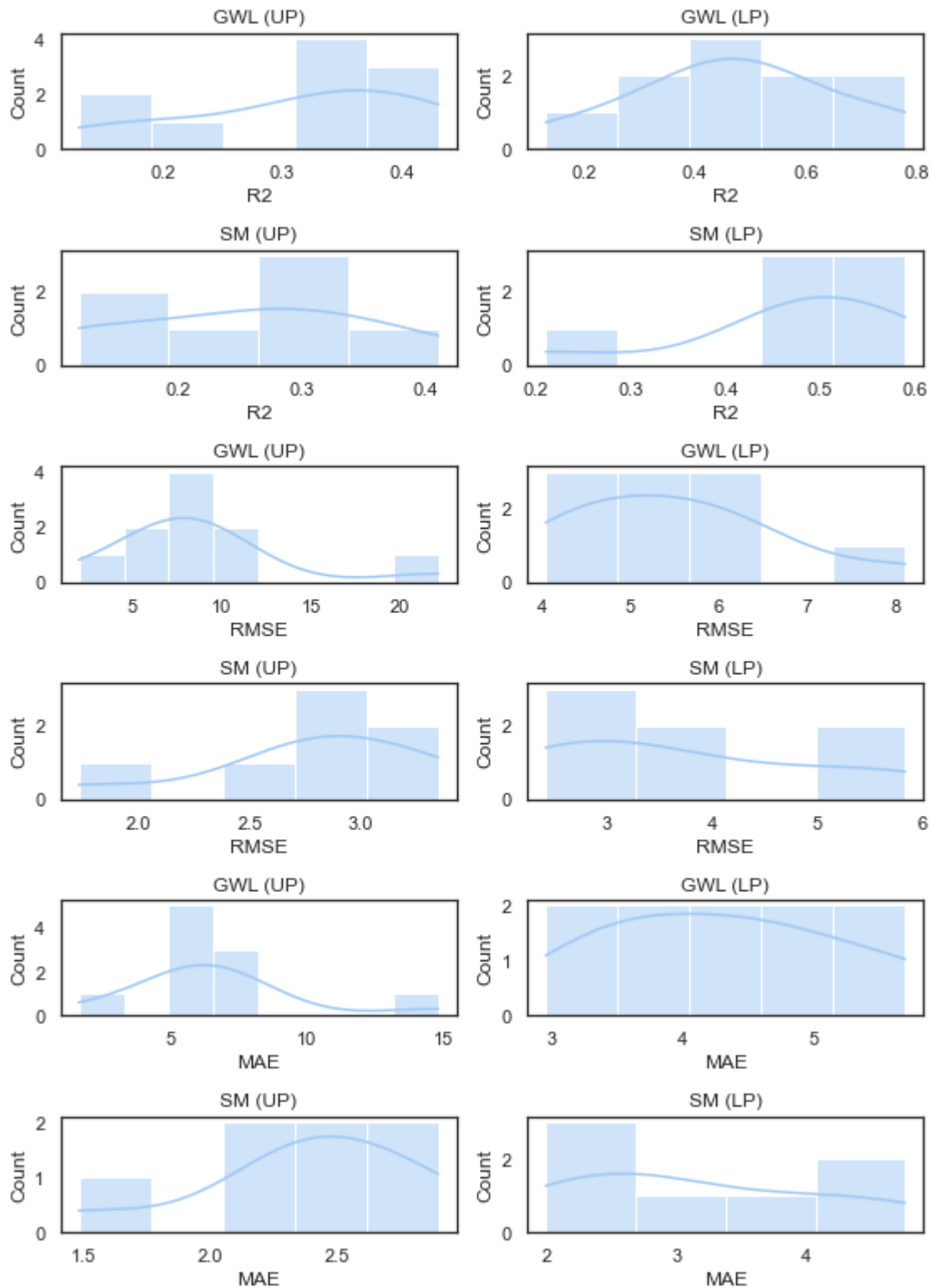
Figure 9. An overview of evaluating metrics including Squared Pearson correlation (R^2), Root Mean Square Error (RMSE), and Mean Absolute Error (MAE) between in-situ data such as Groundwater Level (GWL) and Soil Moisture (SM) for the Upper Part (UP) and Lower Part (LP) of the peat bog study area, based on classification of the CAST model after Meyer et al. (2018).

On the one hand, we speculate that the incomplete spatial coverage of the mapping area and hence the incomplete coverage of the UAV maps may have contributed to lower performance due to technical

issues with the drone, cameras (particularly MS and TIR sensor), batteries, or weather conditions (e.g., strong winds around 21 km/h) during the surveys could not be maintained entirely. While modeling, this missing parts of a partly missing MS map (NDVI variable) or TIR map (temperature variable) affected the model predictions and thus created gaps with missing information. On the other hand, among the essential variables were those that do not lead to an over-fitting and are more focused on model performance in the context of unknown space locations or time steps (Meyer et al., 2018), which were suggested yielding optimal results in view to LLO. Removing misinterpreted variables, such as temporally constant predictors (e.g., elevation, slope, …), could not improve the performance, suggesting that the variables' potential to predict beyond the training locations and time is weakened. However, the models are more robust as only a small subsidy of the initial variables was used. Others were rated as counterproductive and had been removed during FFS, and over-fitting could be reduced. Though predicting environmental variables in space and time remains challenging, the validation strategy used here allows for assessing model errors objectively and identifying over-fitting. However, it should be treated with caution because the relationships between these variables and GWL and SM are complex (Reus, 2022). Nevertheless, this study showed that defining and visualizing the AOA for a spatial prediction model helps ensure high-quality predictions. The AOA is a crucial part of the spatially explicit mapping error estimation. It can depict where the estimated model performance can be expected to hold because the model was enabled to learn about such environments. The AOA can further provide new insight into missing training data and whether new sampling is needed to adequately represent the entire prediction domain (Ludwig et al., 2022).

6. Conclusions and outlook

The dissertation demonstrated that UAV-based photogrammetry and image analysis techniques can be used for non-invasive, objective, and accurate determination of a range of parameters important for understanding the changing dynamics of hydrological and physiographic processes and determining their response to changing climate. My research aimed to develop and demonstrate the potential of novel techniques that allow the use of UAV-based technologies to extract various parameters, including SD, LAI, PSD, river sustainability, river bathymetry, and microclimatic variables related to morphology, topography, vegetation, and temperature.

Papers I and III contributed as follows:

- The studies found that it is possible to achieve satisfactory results using RGB-based UAV imagery for estimating SD and indirect winter LAI_{eff} even under unfavorable conditions such as overcast or partly cloudy weather and insufficient illumination. However, to achieve accurate estimates of SD and indirect winter LAI_{eff}, it is crucial to ensure good illumination during the survey. This is because flying the UAV under good illumination of the surveyed area can help to create a better SD model, which will, in turn, improve the accuracy of the estimates of SD and indirect winter LAI_{eff}, especially in cases where there is no snow interception or no snow-covered wood at the ground for the latter. Further work is needed to simultaneously extract SD and forest structure information to effectively substitute time-consuming fieldwork for delivering direct input data for empirical models in snow research. The next step will be to assess SWE using UAV-mounted radar and perform initial field experiments to complete the suite of snowpack parameters using UAV RS.

Papers II and V contributed as follows:
- The studies proposed novel techniques with significant advantages over traditional granulometric surveys: greater flexibility across multiple study sites and the potential for multitemporal analysis of areas undergoing significant granulometric changes at different time horizons, including changes due to weather events over time. The ultra-high resolution of orthoimages provides more detailed information, which helps estimate local effects on river bars, and allows for analysis in variable user-defined patterns independent of the design of the file sampling campaign. This enables researchers to design and test different patterns for granulometric analysis according to the goals of their studies. However, the DL approach is limited because it does not quickly transfer scales to new data, requiring significant effort and

time to train the model for a new setting. A training-free image processing tool like BASEGRAIN (Detert & Weitbrecht, 2012) could replace the manual annotation process, making the process more efficient and reducing the effort required to train the model in the future.

Paper IV contributed as follows:
- The study demonstrated a framework for using the RF ML algorithm, LLO CV, and multisensor UAV imagery (RGB, MS, TIR) to identify critical microclimatic variables that control and govern GWL and SM in peatlands with moderate accuracy. The FFS method prevented overfitting, and only the optimal predictor variables were used for spatial and temporal model predictions. Additionally, the AOA was applied to limit predictions to the spatial area that features an environment that the model was enabled to learn about, suggesting that assessing the AOA is essential to avoid wrong conclusions and increase the quality of ML based on fieldwork data. The study demonstrated the importance of careful planning and a modern mapping approach to extend results from point locations to the test plots. However, given the highly dynamic nature of the environment, the study also highlighted the need for caution in interpreting snapshot measurements and the potential limitations of using limited field samples to train models for mapping more prominent areas.

Paper VI contributed as follows:
- The study found that although the primary goals of the restoration projects were achieved, the new steam patterns significantly differed from the approved restoration plans. The restored channels were less complex. They featured a simpler geometry than planned, leading to a deficit in the complexity of the realized restorations, which deteriorates the positive effect of the projects and limits their sustainability. In addition, UAV monitoring indicated substantial shortcomings in the qualitative aspects of the restorations in streams and riparian zones. The study highlighted the importance of the conjoint assessment of quantitative and qualitative aspects of stream restoration projects. The use of UAV monitoring and optical RGB sensors has the potential to provide reliable and feature-rich spatial information, enabling the assessment of the critical geometric and qualitative aspects of stream restorations.

Paper VII contributed as follows:
- The main findings were that the approach is practical for bottom topography reconstruction, primarily when multi-rotors are utilized. The resulting higher errors associated with fixed-wing acquisition can be affected by the vulnerability of this platform to the wind. The study also found that bottom river reconstruction decimeter levels were obtained for only 25% of cases for all sites and platforms. The results varied depending on the site and the type of platform. The analyzed method was repeatable and reproducible, especially for multi-rotors. The conclusion is that using the SfM algorithm and the refractive index, the river bottom reconstruction method is robust, especially regarding its repeatability and reproducibility.

7. References

Agisoft LLC. Available online: https://www.agisoft.com/pdf/metashape-pro_1_7_en.pdf (accessed on 15 September 2021).

Aasen, H., & Bolten, A. (2018). Multi-temporal high-resolution imaging spectroscopy with hyperspectral 2D imagers – From theory to application. *Remote Sensing of Environment*, *205*, 374–389. https://doi.org/10.1016/j.rse.2017.10.043

Aasen, H., Burkart, A., Bolten, A., & Bareth, G. (2015). Generating 3D hyperspectral information with lightweight UAV snapshot cameras for vegetation monitoring: From camera calibration to quality assurance. *ISPRS Journal of Photogrammetry and Remote Sensing*, *108*, 245–259. https://doi.org/10.1016/j.isprsjprs.2015.08.002

Adams, M. S., Bühler, Y., & Fromm, R. (2018a). Multitemporal Accuracy and Precision Assessment of Unmanned Aerial System Photogrammetry for Slope-Scale Snow Depth Maps in Alpine Terrain. *Pure and Applied Geophysics*, *175*(9), 3303–3324. https://doi.org/10.1007/s00024-017-1748-y

Adams, M. S., Bühler, Y., & Fromm, R. (2018b). Multitemporal Accuracy and Precision Assessment of Unmanned Aerial System Photogrammetry for Slope-Scale Snow Depth Maps in Alpine Terrain. *Pure and Applied Geophysics*, *175*(9), 3303–3324. https://doi.org/10.1007/s00024-017-1748-y

Ahmed, E., Arshad, M., Khan, M. Z., Amjad, M. S., Sadaf, H. M., Riaz, I., Sabir, S., Ahmad, N., & Sabaoon. (2017). Secondary metabolites and their multidimensional prospective in plant life. *Journal of Pharmacognosy and Phytochemistry*, *6*(2), 205–214.

Assmann, J. J., Kerby, J. T., Cunliffe, A. M., & Myers-Smith, I. H. (2019). Vegetation monitoring using multispectral sensors—Best practices and lessons learned from high latitudes. *Journal of Unmanned Vehicle Systems*, *7*(1), 54–75. https://doi.org/10.1139/juvs-2018-0018

Avanzi, F., Bianchi, A., Cina, A., De Michele, C., Maschio, P., Pagliari, D., Passoni, D., Pinto, L., Piras, M., & Rossi, L. (2017). Measuring the snowpack depth with Unmanned Aerial System photogrammetry: Comparison with manual probing and a 3D laser scanning over a sample plot. *The Cryosphere Discussions*, 1–19. https://doi.org/10.5194/tc-2017-57

Avanzi, F., Bianchi, A., Cina, A., De Michele, C., Maschio, P., Pagliari, D., Passoni, D., Pinto, L., Piras, M., & Rossi, L. (2018a). Centimetric Accuracy in Snow Depth Using Unmanned Aerial System Photogrammetry and a MultiStation. *Remote Sensing*, *10*(5), Article 5. https://doi.org/10.3390/rs10050765

Avanzi, F., Bianchi, A., Cina, A., De Michele, C., Maschio, P., Pagliari, D., Passoni, D., Pinto, L., Piras, M., & Rossi, L. (2018b). Centimetric Accuracy in Snow Depth Using Unmanned Aerial System Photogrammetry and a MultiStation. *Remote Sensing*, *10*(5), 765. https://doi.org/10.3390/rs10050765

Baker Jr., M. B. (1986). Effects of Ponderosa Pine Treatments on Water Yield in Arizona. *Water Resources Research*, *22*(1), 67–73. https://doi.org/10.1029/WR022i001p00067

Balasubramanian, A. (2010). *Fluvial processes and landforms*. Technical Report.

Bandini, F., Butts, M., Jacobsen, T. V., & Bauer-Gottwein, P. (2017). Water level observations from unmanned aerial vehicles for improving estimates of surface water–groundwater interaction. *Hydrological Processes*, *31*(24), 4371–4383. https://doi.org/10.1002/hyp.11366

Barnett, T. P., Dümenil, L., Schlese, U., Roeckner, E., & Latif, M. (1989). The effect of Eurasian snow cover on regional and global climate variations. *Journal of the Atmospheric Sciences*, *46*(5), 661–686.

Battin, T. J., Lauerwald, R., Bernhardt, E. S., Bertuzzo, E., Gener, L. G., Hall Jr, R. O., Hotchkiss, E. R., Maavara, T., Pavelsky, T. M., & Ran, L. (2023). River ecosystem metabolism and carbon biogeochemistry in a changing world. *Nature*, *613*(7944), 449–459.

Belmonte, A., Sankey, T., Biederman, J., Bradford, J., Goetz, S., & Kolb, T. (2021). UAV-Based Estimate of Snow Cover Dynamics: Optimizing Semi-Arid Forest Structure for Snow Persistence. *Remote Sensing*, *13*(5), Article 5. https://doi.org/10.3390/rs13051036

Berni, J., Zarco-Tejada, P., Suárez, L., González-Dugo, V., & Fereres, E. (2009). *REMOTE SENSING*

OF VEGETATION FROM UAV PLATFORMS USING LIGHTWEIGHT MULTISPECTRAL AND THERMAL IMAGING SENSORS. https://www.semanticscholar.org/paper/REMOTE-SENSING-OF-VEGETATION-FROM-UAV-PLATFORMS-AND-Berni-Zarco-Tejada/41e484a1da2dd13357273888429d8eb338ee3724

Beyer, F., Jurasinski, G., Couwenberg, J., & Grenzdörffer, G. (2019). Multisensor data to derive peatland vegetation communities using a fixed-wing unmanned aerial vehicle. *International Journal of Remote Sensing*, *40*(24), 9103–9125. https://doi.org/10.1080/01431161.2019.1580825

Bhardwaj, A., Sam, L., Martín-Torres, F. J., & Kumar, R. (2016). UAVs as remote sensing platform in glaciology: Present applications and future prospects. *Remote sensing of environment*, *175*, 196–204.

Boesch, R. (2017). Thermal remote sensing with UAV-based workflows. *The International Archives of the Photogrammetry, Remote Sensing and Spatial Information Sciences*, *42*, 41-46. https://doi.org/10.5194/isprs-archives-XLII-2-W6-41-2017, 2017.

Brigante, R., Cencetti, C., De Rosa, P., Fredduzzi, A., Radicioni, F., & Stoppini, A. (2017). Use of aerial multispectral images for spatial analysis of flooded riverbed-alluvial plain systems: The case study of the Paglia River (central Italy). *Geomatics, Natural Hazards and Risk*, *8*(2), 1126–1143. https://doi.org/10.1080/19475705.2017.1300607

Briscoe, N. J., Handasyde, K. A., Griffiths, S. R., Porter, W. P., Krockenberger, A., & Kearney, M. R. (2014). Tree-hugging koalas demonstrate a novel thermoregulatory mechanism for arboreal mammals. *Biology Letters*, *10*(6), 20140235. https://doi.org/10.1098/rsbl.2014.0235

Brocca, L., Ciabatta, L., Massari, C., Camici, S., & Tarpanelli, A. (2017). Soil Moisture for Hydrological Applications: Open Questions and New Opportunities. *Water*, *9*(2), Article 2. https://doi.org/10.3390/w9020140

Budzier, H., & Gerlach, G. (2015). Calibration of uncooled thermal infrared cameras. *Journal of Sensors and Sensor Systems*, *4*(1), 187–197. https://doi.org/10.5194/jsss-4-187-2015

Bugmann, H., Gurung, A. B., Ewert, F., Haeberli, W., Guisan, A., Fagre, D., & Kääb, A. (2007). Modeling the biophysical impacts of global change in mountain biosphere reserves. *Mountain Research and Development*, *27*(1), 66–77.

Bühler, Y., Adams, M. S., Bösch, R., & Stoffel, A. (2016). Mapping snow depth in alpine terrain with unmanned aerial systems (UASs): Potential and limitations. *The Cryosphere*, *10*(3), 1075–1088. https://doi.org/10.5194/tc-10-1075-2016

Bunte, K., & Abt, S. R. (2001). Sampling Frame for Improving Pebble Count Accuracy in Coarse Gravel-Bed Streams1. *JAWRA Journal of the American Water Resources Association*, *37*(4), 1001–1014. https://doi.org/10.1111/j.1752-1688.2001.tb05528.x

Buscombe, D. (2013). Transferable wavelet method for grain‑size distribution from images of sediment surfaces and thin sections, and other natural granular patterns. *Sedimentology*, *60*, 1709–1732. https://doi.org/10.1111/SED.12049

Butler, J. B., Lane, S. N., & Chandler, J. H. (2001). Automated extraction of grain-size data from gravel surfaces using digital image processing. *Journal of Hydraulic Research*, *39*(5), 519–529. https://doi.org/10.1080/00221686.2001.9628276

Camenen, B., Herrero, A., Dramais, G., Thollet, F., Bescond, C. L., Perret, E., Camenen, B., Herrero, A., Dramais, G., Thollet, F., Bescond, C. L., Perret, E., & Berni, C. (2016). Field experiment on the dynamics of fine sediments over a gravel bar in an alpine gravel-bed river. *9th Symposium on River, Coastal and Estuarine Morphodynamics*, 6.

Chasmer, L., Mahoney, C., Millard, K., Nelson, K., Peters, D., Merchant, M., Hopkinson, C., Brisco, B., Niemann, O., Montgomery, J., Devito, K., & Cobbaert, D. (2020). Remote Sensing of Boreal Wetlands 2: Methods for Evaluating Boreal Wetland Ecosystem State and Drivers of Change. *Remote Sensing*, *12*(8), Article 8. https://doi.org/10.3390/rs12081321

Chianucci, F., & Cutini, A. (2012). Digital hemispherical photography for estimating forest canopy properties: Current controversies and opportunities. *IForest*, *5*(6), 290–295. https://doi.org/10.3832/ifor0775-005

Cimoli, E. (2015). Determining Snow Depth Distribution from Unmanned Aerial Vehicles and Digital Photogrammetry. *MSc Thesis*, *Technical*.

Cimoli, E., Marcer, M., Vandecrux, B., Bøggild, C. E., Williams, G., & Simonsen, S. B. (2017). Application of Low-Cost UASs and Digital Photogrammetry for High-Resolution Snow Depth Mapping in the Arctic. *Remote Sensing*, *9*(11), 1144. https://doi.org/10.3390/rs9111144

Colomina, I., & Molina, P. (2014). Unmanned aerial systems for photogrammetry and remote sensing: A review. *ISPRS Journal of Photogrammetry and Remote Sensing*, *92*, 79–97. https://doi.org/10.1016/j.isprsjprs.2014.02.013

Cooper, H. M., Wasklewicz, T., Zhu, Z., Lewis, W., LeCompte, K., Heffentrager, M., Smaby, R., Brady, J., & Howard, R. (2021). Evaluating the Ability of Multi-Sensor Techniques to Capture Topographic Complexity. *Sensors*, *21*(6), Article 6. https://doi.org/10.3390/s21062105

Crusiol, L. G. T., Nanni, M. R., Silva, G. F. C., Furlanetto, R. H., da Silva Gualberto, A. A., Gasparotto, A. de C., & De Paula, M. N. (2017). Semi professional digital camera calibration techniques for Vis/NIR spectral data acquision from an unmanned aerial vehicle. *International Journal of Remote Sensing*, *38*(8–10), 2717–2736. https://doi.org/10.1080/01431161.2016.1264032

Cruzan, M. B., Weinstein, B. G., Grasty, M. R., Kohrn, B. F., Hendrickson, E. C., Arredondo, T. M., & Thompson, P. G. (2016). Small unmanned aerial vehicles (micro-UAVs, drones) in plant ecology. *Applications in Plant Sciences*, *4*(9), apps.1600041. https://doi.org/10.3732/apps.1600041

Curda, J., Jansky, B., & Kocum, J. (2011). The effects of physical-geographic factors on flood episodes extremity in the Vydra River basin. *Geografie*, *116*(3), 335–353.

Currier, W. R., Pflug, J., Mazzotti, G., Jonas, T., Deems, J. S., Bormann, K. J., Painter, T. H., Hiemstra, C. A., Gelvin, A., Uhlmann, Z., Spaete, L., Glenn, N. F., & Lundquist, J. D. (2019). Comparing Aerial Lidar Observations With Terrestrial Lidar and Snow-Probe Transects From NASA's 2017 SnowEx Campaign. *Water Resources Research*, *55*(7), 6285–6294. https://doi.org/10.1029/2018WR024533

Dai, L., Fu, R., Guo, X., Du, Y., Zhang, F., & Cao, G. (2022). Soil Moisture Variations in Response to Precipitation Across Different Vegetation Types on the Northeastern Qinghai-Tibet Plateau. *Frontiers in Plant Science*, *13*. https://www.frontiersin.org/articles/10.3389/fpls.2022.854152

Damm, A., Cogliati, S., Colombo, R., Fritsche, L., Genangeli, A., Genesio, L., Hanus, J., Peressotti, A., Rademske, P., Rascher, U., Schuettemeyer, D., Siegmann, B., Sturm, J., & Miglietta, F. (2022). Response times of remote sensing measured sun-induced chlorophyll fluorescence, surface temperature and vegetation indices to evolving soil water limitation in a crop canopy. *Remote Sensing of Environment*, *273*, 112957. https://doi.org/10.1016/j.rse.2022.112957

De Michele, C., Avanzi, F., Passoni, D., Barzaghi, R., Pinto, L., Dosso, P., Ghezzi, A., Gianatti, R., & Vedova, G. D. (2016). Using a fixed-wing UAS to map snow depth distribution: An evaluation at peak accumulation. *Cryosphere*, *10*(2), 511–522. https://doi.org/10.5194/tc-10-511-2016

Deems, J. S., & Painter, T. H. (2014). *Airborne LiDAR and hyperspectral mapping of snow depth and albedo in the Upper Colorado River Basin, Colorado, USA by the NASA JPL Airborne Snow Observatory*. *2014*, C43D-0413.

Deems, J. S., Painter, T. H., & Finnegan, D. C. (2013). Lidar measurement of snow depth: A review. *Journal of Glaciology*, *59*(215), 467–479. https://doi.org/10.3189/2013JoG12J154

Deschamps-Berger, C., Gascoin, S., Berthier, E., Deems, J., Gutmann, E., Dehecq, A., Shean, D., & Dumont, M. (2020). Snow depth mapping from stereo satellite imagery in mountainous terrain: Evaluation using airborne laser-scanning data. *The Cryosphere*, *14*(9), 2925–2940. https://doi.org/10.5194/tc-14-2925-2020

Detert, M., & Weitbrecht, V. (2012). Automatic object detection to analyze the geometry of gravel grains–a free stand-alone tool. *River Flow 2012, August 2016*, 595–600.

Dinsmore, K. J., Skiba, U. M., Billett, M. F., & Rees, R. M. (2008). Effect of water table on greenhouse gas emissions from peatland mesocosms. *Plant and Soil*, *318*(1), 229. https://doi.org/10.1007/s11104-008-9832-9

Du, M., & Noguchi, N. (2017). Monitoring of wheat growth status and mapping of wheat yield's within-field spatial variations using color images acquired from UAV-camera system. *Remote sensing*, *9*(3), 289. https://doi.org/10.3390/rs9030289

Eberhard, L. A., Sirguey, P., Miller, A., Marty, M., Schindler, K., Stoffel, A., & Bühler, Y. (2021).

Intercomparison of photogrammetric platforms for spatially continuous snow depth mapping. *The Cryosphere*, *15*(1), 69–94. https://doi.org/10.5194/tc-15-69-2021

Ecke, S., Dempewolf, J., Frey, J., Schwaller, A., Endres, E., Klemmt, H.-J., Tiede, D., & Seifert, T. (2022). UAV-Based Forest Health Monitoring: A Systematic Review. *Remote Sensing*, *14*(13), Article 13. https://doi.org/10.3390/rs14133205

Eker, R., & Aydın, A. (o. J.). *Evaluation of snow avalanche hazard on the highway using high resolution UAV data: Case of the Erzurum-Çat-Karlıova highway, Turkey*.

Fenner, N., & Freeman, C. (2011). Drought-induced carbon loss in peatlands. *Nature Geoscience*, *4*(12), Article 12. https://doi.org/10.1038/ngeo1323

Ferguson, R. I., Lewin, J., & Hardy, R. J. (2022). Fluvial processes and landforms. *Geological Society, London, Memoirs*, *58*(1), 257–270.

Fernandes, R., Prevost, C., Canisius, F., Leblanc, S. G., Maloley, M., Oakes, S., Holman, K., & Knudby, A. (2018). Monitoring snow depth change across a range of landscapes with ephemeral snowpacks using structure from motion applied to lightweight unmanned aerial vehicle videos. *The Cryosphere*, *12*(11), 3535–3550. https://doi.org/10.5194/tc-12-3535-2018

Figueiredo, P. M., & Rockwell, T. K. (2022). 2.17—Application of Coastal Landforms to Active Tectonic Studies. In J. (Jack) F. Shroder (Hrsg.), *Treatise on Geomorphology (Second Edition)* (S. 443–476). Academic Press. https://doi.org/10.1016/B978-0-12-818234-5.00163-2

Flener, C., Vaaja, M., Jaakkola, A., Krooks, A., Kaartinen, H., Kukko, A., Kasvi, E., Hyyppä, H., Hyyppä, J., & Alho, P. (2013). Seamless mapping of river channels at high resolution using mobile liDAR and UAV-photography. *Remote Sensing*, *5*(12), 6382–6407. https://doi.org/10.3390/rs5126382

Fonstad, M. A., Dietrich, J. T., Courville, B. C., Jensen, J. L., & Carbonneau, P. E. (2013). Topographic structure from motion: A new development in photogrammetric measurement: TOPOGRAPHIC STRUCTURE FROM MOTION. *Earth Surface Processes and Landforms*, *38*(4), 421–430. https://doi.org/10.1002/esp.3366

Fountain, A. G., Campbell, J. L., Schuur, E. A., Stammerjohn, S. E., Williams, M. W., & Ducklow, H. W. (2012). The disappearing cryosphere: Impacts and ecosystem responses to rapid cryosphere loss. *BioScience*, *62*(4), 405–415.

Gehrke, S., Morin, K., Downey, M., Boehrer, N., & Fuchs, T. (2010, June). Semi-global matching: An alternative to LIDAR for DSM generation. In *Proceedings of the 2010 Canadian Geomatics Conference and Symposium of Commission I* (Vol. 2, No. 6).

Gerhards, M., Schlerf, M., Mallick, K., & Udelhoven, T. (2019). Challenges and Future Perspectives of Multi-/Hyperspectral Thermal Infrared Remote Sensing for Crop Water-Stress Detection: A Review. *Remote Sensing*, *11*(10), Article 10. https://doi.org/10.3390/rs11101240

Giordano, F., Mattei, G., Parente, C., Peluso, F., & Santamaria, R. (2016). Integrating Sensors into a Marine Drone for Bathymetric 3D Surveys in Shallow Waters. *Sensors*, *16*(1), Article 1. https://doi.org/10.3390/s16010041

Gleason, K. E., Nolin, A. W., & Roth, T. R. (2017). Developing a representative snow-monitoring network in a forested mountain watershed. *Hydrology and Earth System Sciences*, *21*(2), 1137–1147. https://doi.org/10.5194/hess-21-1137-2017

Goetz, J., Brenning, A., Marcer, M., & Bodin, X. (2018). Modeling the precision of structure-from-motion multi-view stereo digital elevation models from repeated close-range aerial surveys. *Remote Sensing of Environment*, *210*, 208–216. https://doi.org/10.1016/j.rse.2018.03.013

Grabowski, R. C., Vercruysse, K., Holman, I., Azhoni, A., Bala, B., Shankar, V., Beale, J., Mukate, S., Poddar, A., Peng, J., & Meersmans, J. (2022). The land–river interface: A conceptual framework of environmental process interactions to support sustainable development. *Sustainability Science*, *17*(4), 1677–1693. https://doi.org/10.1007/s11625-022-01150-x

Graham, D., Rice, S., & Reid, I. (2005). *Comment: Photographic Techniques for Characterizing Streambed Particle Sizes*. https://doi.org/10.1577/T04-146.1

Granshaw, S. (1980). Bundle adjustment methods in engineering photogrammetry. *The Photogrammetric Record*, *10*(56), 181–207.

Granshaw, S. I. (2020). Photogrammetric terminology: Fourth edition. *The Photogrammetric Record*, *35*(170), 143–288. https://doi.org/10.1111/phor.12314

Grau-Andrés, R., Gray, A., Davies, G. M., Scott, E. M., & Waldron, S. (2019). Burning increases post-fire carbon emissions in a heathland and a raised bog, but experimental manipulation of fire severity has no effect. *Journal of Environmental Management*, *233*, 321–328. https://doi.org/10.1016/j.jenvman.2018.12.036

Grayson, R. B., Moore, I. D., & McMahon, T. A. (1992a). Physically based hydrologic modeling: 1. A terrain-based model for investigative purposes. *Water Resources Research*, *28*(10), 2639–2658. https://doi.org/10.1029/92WR01258

Grayson, R. B., Moore, I. D., & McMahon, T. A. (1992b). Physically based hydrologic modeling: 2. Is the concept realistic? *Water Resources Research*, *28*(10), 2659–2666. https://doi.org/10.1029/92WR01259

Griffiths, D., & Burningham, H. (2019). Comparison of pre- and self-calibrated camera calibration models for UAS-derived nadir imagery for a SfM application. *Progress in Physical Geography: Earth and Environment*, *43*(2), 215–235. https://doi.org/10.1177/0309133318788964

Guan, S., Sirianni, H., Wang, G., & Zhu, Z. (2022). sUAS monitoring of coastal environments: A review of best practices from field to lab. *Drones*, *6*(6), 142. https://doi.org/10.3390/drones6060142

Guo, Y., Senthilnath, J., Wu, W., Zhang, X., Zeng, Z., & Huang, H. (2019). Radiometric calibration for multispectral camera of different imaging conditions mounted on a UAV platform. *Sustainability*, *11*(4), 978.https://doi.org/10.3390/su11040978

Harder, P., Schirmer, M., Pomeroy, J., & Helgason, W. (2016). Accuracy of snow depth estimation in mountain and prairie environments by an unmanned aerial vehicle. *The Cryosphere*, *10*(6), 2559-2571.https://doi.org/10.5194/tc-10-2559-2016

Harris, A., & Baird, A. J. (2019). Microtopographic Drivers of Vegetation Patterning in Blanket Peatlands Recovering from Erosion. *Ecosystems*, *22*(5), 1035–1054. https://doi.org/10.1007/s10021-018-0321-6

HEIS VÚV. (o. J.). Abgerufen 28. Februar 2023, von https://heis.vuv.cz/

Hird, J., DeLancey, E., McDermid, G., & Kariyeva, J. (2017). Google Earth Engine, Open-Access Satellite Data, and Machine Learning in Support of Large-Area Probabilistic Wetland Mapping. *Remote Sensing*, *9*(12), 1315. https://doi.org/10.3390/rs9121315

Hirschmüller, H. (2008). Stereo processing by semiglobal matching and mutual information. *IEEE Transactions on Pattern Analysis and Machine Intelligence*, *30*(2), 328–341. https://doi.org/10.1109/TPAMI.2007.1166

Honkavaara, E., Hakala, T., Markelin, L., Jaakkola, A., Saari, H., Ojanen, H., Pölönen, I., Tuominen, S., Näsi, R., Rosnell, T., & Viljanen, N. (2014). Autonomous hyperspectral UAS photogrammetry for environmental monitoring applications. *The International Archives of the Photogrammetry, Remote Sensing and Spatial Information Sciences*, *XL–1*, 155–159. https://doi.org/10.5194/isprsarchives-XL-1-155-2014

Huang, Y., Ding, W., & Li, H. (2016). Haze removal for UAV reconnaissance images using layered scattering model. *Chinese Journal of Aeronautics*, *29*(2), 502–511. https://doi.org/10.1016/j.cja.2016.01.012

Imran, H. A., Gianelle, D., Rocchini, D., Dalponte, M., Martín, M. P., Sakowska, K., Wohlfahrt, G., & Vescovo, L. (2020). VIS-NIR, Red-Edge and NIR-Shoulder Based Normalized Vegetation Indices Response to Co-Varying Leaf and Canopy Structural Traits in Heterogeneous Grasslands. *Remote Sensing*, *12*(14), Article 14. https://doi.org/10.3390/rs12142254

Jain, A. K. (2010). Data clustering: 50 years beyond K-means. *Pattern recognition letters*, *31*(8), 651–666.

James, M. R., Robson, S., & Smith, M. W. (2017). 3-D uncertainty-based topographic change detection with structure-from-motion photogrammetry: Precision maps for ground control and directly georeferenced surveys. *Earth Surface Processes and Landforms*, *42*(12), 1769–1788. https://doi.org/10.1002/esp.4125

Jeziorska, J. (2019). UAS for Wetland Mapping and Hydrological Modeling. *Remote Sensing*, *11*(17), Article 17. https://doi.org/10.3390/rs11171997

Jonckheere, I., Fleck, S., Nackaerts, K., Muys, B., Coppin, P., Weiss, M., & Baret, F. (2004). Review of methods for in situ leaf area index determination Part I. Theories, sensors and hemispherical photography. *Agricultural and Forest Meteorology*, *121*(1–2), 19–35. https://doi.org/10.1016/j.agrformet.2003.08.027

Jones, P. (2023). Peatland restoration in the UK. *Town and Country Planning*, 47–52.

Jost, G., Dan Moore, R., Smith, R., & Gluns, D. R. (2012). Distributed temperature-index snowmelt modelling for forested catchments. *Journal of Hydrology*, *420–421*, 87–101. https://doi.org/10.1016/j.jhydrol.2011.11.045

Kelcey, J., & Lucieer, A. (2012). Sensor correction of a 6-band multispectral imaging sensor for UAV remote sensing. *Remote Sensing*, *4*(5), 1462–1493. https://doi.org/10.3390/rs4051462

Kelly, J., Kljun, N., Olsson, P.-O., Mihai, L., Liljeblad, B., Weslien, P., Klemedtsson, L., & Eklundh, L. (2019). Challenges and Best Practices for Deriving Temperature Data from an Uncalibrated UAV Thermal Infrared Camera. *Remote Sensing*, *11*(5), 567. https://doi.org/10.3390/rs11050567

Kimmel, K., & Mander, Ü. (2010). Ecosystem services of peatlands: Implications for restoration. *Progress in Physical Geography: Earth and Environment*, *34*(4), 491–514. https://doi.org/10.1177/0309133310365595

Kingma, D. P., & Ba, J. (2017). *Adam: A Method for Stochastic Optimization* (arXiv:1412.6980). arXiv. https://doi.org/10.48550/arXiv.1412.6980

Kinzel, P. J., Legleiter, C. J., Nelson, J. M., Conaway, J., LeWinter, A., Gadomski, P., & Filiano, D. (2019). *Near-field remote sensing of Alaskan Rivers*. Federal Interagency Sedimentation and Hydrologic Modeling Conference (SEDHYD 2019). https://pubs.er.usgs.gov/publication/70203958

Kittel, T. G., Baker, B. B., Higgins, J. V., & Haney, J. C. (2011). Climate vulnerability of ecosystems and landscapes on Alaska's North Slope. *Regional Environmental Change*, *11*, 249–264.

Kizuka, T., Mikami, H., Kameyama, S., Ono, S., & Suzuki, H. (2023). Hydrological environment affects the nutrient retention and runoff function of naturally re-wetted agricultural peatland in lowland river floodplain. *Science of The Total Environment*, *857*, 159483.

Knight, J. (2022). Scientists' warning of the impacts of climate change on mountains. *PeerJ*, *10*, e14253.

Knight, J., & Harrison, S. (o. J.). The sensitivity and evolutionary trajectory of the mountain cryosphere: Implications for mountain geomorphic systems and hazards. *Land Degradation & Development*.

Kolokoussis, P., Karathanassi, V., Rokos, D., Argialas, D., Karageorgis, A. P., & Georgopoulos, D. (2011). Integrating thermal and hyperspectral remote sensing for the detection of coastal springs and submarine groundwater discharges. *International Journal of Remote Sensing*. http://dx.doi.org/10.1080/01431161.2010.533209

Koparan, C., Koc, A. B., Privette, C. V., & Sawyer, C. B. (2018). In Situ Water Quality Measurements Using an Unmanned Aerial Vehicle (UAV) System. *Water*, *10*(3), Article 3. https://doi.org/10.3390/w10030264

Krumbein, W. C., & Pettijohn, F. J. (1939). Manual of Sedimentary Petrography. XIV + 549 pp., 8:o, 265 fig. New York and London 1938, (1939). D. Appleton—Century Company. 8 6.50 (30 s.). *Geologiska Föreningen i Stockholm Förhandlingar*, *61*(2), 225–227. https://doi.org/10.1080/11035893909452786

KUSTAS, W. P., & NORMAN, J. M. (1996). Use of remote sensing for evapotranspiration monitoring over land surfaces. *Hydrological Sciences Journal*, *41*(4), 495–516. https://doi.org/10.1080/02626669609491522

Laliberte, A. S., Goforth, M. A., Steele, C. M., & Rango, A. (2011). Multispectral Remote Sensing from Unmanned Aircraft: Image Processing Workflows and Applications for Rangeland Environments. *Remote Sensing*, *3*(11), Article 11. https://doi.org/10.3390/rs3112529

Lang, N., Irniger, A., Rozniak, A., Hunziker, R., Wegner, J. D., & Schindler, K. (2021). GRAINet: Mapping grain size distributions in river beds from UAV images with convolutional neural networks. *Hydrology and Earth System Sciences*. https://doi.org/10.5194/HESS-25-2567-2021

Langhammer, J., & Vacková, T. (2018). Detection and Mapping of the Geomorphic Effects of Flooding Using UAV Photogrammetry. *Pure and Applied Geophysics*, *175*(9), 3223–3245. https://doi.org/10.1007/s00024-018-1874-1

Lee, S., Hyun, Y., & Lee, M.-J. (2019). Groundwater Potential Mapping Using Data Mining Models of Big Data Analysis in Goyang-si, South Korea. *Sustainability*, *11*(6), 1678. https://doi.org/10.3390/su11061678

Legleiter, C. J., & Kinzel, P. J. (2021). Improving Remotely Sensed River Bathymetry by Image‑Averaging. *Water Resources Research*, *57*(3). https://doi.org/10.1029/2020WR028795

Legleiter, C. J., Overstreet, B. T., & Kinzel, P. J. (2018). Sampling Strategies to Improve Passive Optical Remote Sensing of River Bathymetry. *Remote Sensing*, *10*(6), Article 6. https://doi.org/10.3390/rs10060935

Lejot, J., Delacourt, C., Piégay, H., Fournier, T., Trémélo, M., & Allemand, P. (2007). *Very high spatial resolution imagery for channel bathymetry and topography from an unmanned*. *1725*, 1705–1725. https://doi.org/10.1002/esp

Leng, R., Harrison, S., & Anderson, K. (2022). Himalayan alpine ecohydrology: An urgent scientific concern in a changing climate. *Ambio*, 1–21.

Leopold, L. B., & Wolman, M. G. (1957). *River channel patterns: Braided, meandering, and straight*. US Government Printing Office.

Li, H., Chen, L., Wang, Z., & Yu, Z. (2019). Mapping of River Terraces with Low-Cost UAS Based Structure-from-Motion Photogrammetry in a Complex Terrain Setting. *Remote Sensing*, *11*(4), Article 4. https://doi.org/10.3390/rs11040464

Liu, D., Zhang, C., Ogaya, R., Fernández-Martínez, M., Pugh, T. A. M., & Peñuelas, J. (2021). Increasing climatic sensitivity of global grassland vegetation biomass and species diversity correlates with water availability. *New Phytologist*, *230*(5), 1761–1771. https://doi.org/10.1111/nph.17269

Loisel, J., Gallego-Sala, A. V., Amesbury, M. J., Magnan, G., Anshari, G., Beilman, D. W., Benavides, J. C., Blewett, J., Camill, P., Charman, D. J., Chawchai, S., Hedgpeth, A., Kleinen, T., Korhola, A., Large, D., Mansilla, C. A., Müller, J., van Bellen, S., West, J. B., … Wu, J. (2021). Expert assessment of future vulnerability of the global peatland carbon sink. *Nature Climate Change*, *11*(1), Article 1. https://doi.org/10.1038/s41558-020-00944-0

Loisel, J., Yu, Z., Beilman, D. W., Camill, P., Alm, J., Amesbury, M. J., Anderson, D., Andersson, S., Bochicchio, C., Barber, K., Belyea, L. R., Bunbury, J., Chambers, F. M., Charman, D. J., De Vleeschouwer, F., Fiałkiewicz-Kozieł, B., Finkelstein, S. A., Gałka, M., Garneau, M., … Zhou, W. (2014). A database and synthesis of northern peatland soil properties and Holocene carbon and nitrogen accumulation. *The Holocene*, *24*(9), 1028–1042. https://doi.org/10.1177/0959683614538073

Lovitt, J., Rahman, M. M., Saraswati, S., McDermid, G. J., Strack, M., & Xu, B. (2018). UAV Remote Sensing Can Reveal the Effects of Low-Impact Seismic Lines on Surface Morphology, Hydrology, and Methane (CH_4) Release in a Boreal Treed Bog. *Journal of Geophysical Research: Biogeosciences*, *123*(3), 1117–1129. https://doi.org/10.1002/2017JG004232

Ludwig, M., Bahlmann, J., Pebesma, E., & Meyer, H. (2022). DEVELOPING TRANSFERABLE SPATIAL PREDICTION MODELS: A CASE STUDY OF SATELLITE BASED LANDCOVER MAPPING. *The International Archives of the Photogrammetry, Remote Sensing and Spatial Information Sciences*, *XLIII-B3-2022*, 135–141. https://doi.org/10.5194/isprs-archives-XLIII-B3-2022-135-2022

Lundquist, J. D., Dickerson-Lange, S. E., Lutz, J. A., & Cristea, N. C. (2013). Lower forest density enhances snow retention in regions with warmer winters: A global framework developed from plot-scale observations and modeling: Forests and Snow Retention. *Water Resources Research*, *49*(10), 6356–6370. https://doi.org/10.1002/wrcr.20504

Malekzadeh, M., Kardar, S., Saeb, K., Shabanlou, S., & Taghavi, L. (2019). A Novel Approach for Prediction of Monthly Ground Water Level Using a Hybrid Wavelet and Non-Tuned Self-Adaptive Machine Learning Model. *Water Resources Management*, *33*(4), 1609–1628. https://doi.org/10.1007/s11269-019-2193-8

Marti, R., Gascoin, S., Berthier, E., de Pinel, M., Houet, T., & Laffly, D. (2016). Mapping snow depth in open alpine terrain from stereo satellite imagery. *The Cryosphere*, *10*(4), 1361–1380. https://doi.org/10.5194/tc-10-1361-2016

Martínez Prentice, R., Villoslada Peciña, M., Ward, R. D., Bergamo, T. F., Joyce, C. B., & Sepp, K. (2021). Machine Learning Classification and Accuracy Assessment from High-Resolution Images of Coastal Wetlands. *Remote Sensing*, *13*(18), Article 18. https://doi.org/10.3390/rs13183669

Mayer, C., Pereira, L. G., & Kersten, T. P. (2018). *A comprehensive workflow to process UAV images for the efficient production of accurate geo-information*. 1–8.

Mazzotti, G., Essery, R., Moeser, C. D., & Jonas, T. (2020). Resolving Small-Scale Forest Snow Patterns Using an Energy Balance Snow Model With a One-Layer Canopy. *Water Resources Research*, *56*(1), e2019WR026129. https://doi.org/10.1029/2019WR026129

Mazzotti, G., Malle, J., Barr, S., & Jonas, T. (2019). Spatially Continuous Characterization of Forest Canopy Structure and Subcanopy Irradiance Derived from Handheld Radiometer Surveys. *Journal of Hydrometeorology*, *20*(7), 1417–1433. https://doi.org/10.1175/JHM-D-18-0158.1

Mesas-Carrascosa, F.-J., Pérez-Porras, F., Meroño de Larriva, J. E., Mena Frau, C., Agüera-Vega, F., Carvajal-Ramírez, F., Martínez-Carricondo, P., & García-Ferrer, A. (2018). Drift Correction of Lightweight Microbolometer Thermal Sensors On-Board Unmanned Aerial Vehicles. *Remote Sensing*, *10*(4), Article 4. https://doi.org/10.3390/rs10040615

Meyer, H., & Pebesma, E. (2020). Predicting into unknown space? Estimating the area of applicability of spatial prediction models. *ArXiv:2005.07939 [Cs, Stat]*. http://arxiv.org/abs/2005.07939

Meyer, H., Reudenbach, C., Hengl, T., Katurji, M., & Nauss, T. (2018). Improving performance of spatio-temporal machine learning models using forward feature selection and target-oriented validation. *Environmental Modelling & Software*, *101*, 1–9.

Meyer, H., Reudenbach, C., Wöllauer, S., & Nauss, T. (2019). Importance of spatial predictor variable selection in machine learning applications – Moving from data reproduction to spatial prediction. *Ecological Modelling*, *411*, 108815. https://doi.org/10.1016/j.ecolmodel.2019.108815

Miller, J. B. (1967). A formula for average foliage density. *Australian Journal of Botany*, *15*(1), 141–144. https://doi.org/10.1071/bt9670141

Milner, A. M., Khamis, K., Battin, T. J., Brittain, J. E., Barrand, N. E., Füreder, L., Cauvy-Fraunié, S., Gíslason, G. M., Jacobsen, D., & Hannah, D. M. (2017). Glacier shrinkage driving global changes in downstream systems. *Proceedings of the National Academy of Sciences*, *114*(37), 9770–9778.

Minařík, R., & Langhammer, J. (2016). USE OF A MULTISPECTRAL UAV PHOTOGRAMMETRY FOR DETECTION AND TRACKING OF FOREST DISTURBANCE DYNAMICS. *ISPRS - International Archives of the Photogrammetry, Remote Sensing and Spatial Information Sciences*, *XLI-B8*, 711–718. https://doi.org/10.5194/isprsarchives-XLI-B8-711-2016

Minařík, R., Langhammer, J., & Hanuš, J. (2019). Radiometric and Atmospheric Corrections of Multispectral μMCA Camera for UAV Spectroscopy. *Remote Sensing*, *11*(20), 2428. https://doi.org/10.3390/rs11202428

Molotch, N. P., Brooks, P. D., Burns, S. P., Litvak, M., Monson, R. K., McConnell, J. R., & Musselman, K. (2009). Ecohydrological controls on snowmelt partitioning in mixed-conifer sub-alpine forests. *Ecohydrology*, *2*(2), 129–142. https://doi.org/10.1002/eco.48

Morgan, B. J., Stocker, M. D., Valdes-Abellan, J., Kim, M. S., & Pachepsky, Y. (2020). Drone-based imaging to assess the microbial water quality in an irrigation pond: A pilot study. *Science of The Total Environment*, *716*, 135757. https://doi.org/10.1016/j.scitotenv.2019.135757

Morillas, L., García, M., Nieto, H., Villagarcia, L., Sandholt, I., Gonzalez-Dugo, M. P., Zarco-Tejada, P. J., & Domingo, F. (2013). Using radiometric surface temperature for surface energy flux estimation in Mediterranean drylands from a two-source perspective. *Remote Sensing of Environment*, *136*, 234–246. https://doi.org/10.1016/j.rse.2013.05.010

Naghibi, S. A., Ahmadi, K., & Daneshi, A. (2017). Application of Support Vector Machine, Random Forest, and Genetic Algorithm Optimized Random Forest Models in Groundwater Potential Mapping. *Water Resources Management*, *31*(9), 2761–2775. https://doi.org/10.1007/s11269-017-1660-3

Nieto, H., Alsina, M. M., Kustas, W. P., García-Tejera, O., Chen, F., Bambach, N., Gao, F., Alfieri, J. G.,

Hipps, L. E., Prueger, J. H., McKee, L. G., Zahn, E., Bou-Zeid, E., McElrone, A. J., Castro, S. J., & Dokoozlian, N. (2022). Evaluating different metrics from the thermal-based two-source energy balance model for monitoring grapevine water stress. *Irrigation Science*, *40*(4), 697–713. https://doi.org/10.1007/s00271-022-00790-2

Nijp, J. J., Metselaar, K., Limpens, J., Teutschbein, C., Peichl, M., Nilsson, M. B., Berendse, F., & van der Zee, S. E. A. T. M. (2017). Including hydrological self-regulating processes in peatland models: Effects on peatmoss drought projections. *Science of The Total Environment*, *580*, 1389–1400. https://doi.org/10.1016/j.scitotenv.2016.12.104

Nolan, M., Larsen, C., & Sturm, M. (2015). Mapping snow-depth from manned-aircraft on landscape scales at centimeter resolution using Structure-from-Motion photogrammetry. *The Cryosphere Discussions*, *9*, 333–381. https://doi.org/10.5194/tcd-9-333-2015

Olbrycht, R., & Więcek, B. (2014). *New approach to thermal drift correction and gain determination in microbolometer thermal cameras*. https://www.semanticscholar.org/paper/New-approach-to-thermal-drift-correction-and-gain-Olbrycht-Wi%C4%99cek/8b754934b795ed0731d63cf81ad7aed9edd84c0a

Orru, M., Ots, K., & Orru, H. (2016). Re-vegetation processes in cutaway peat production fields in Estonia in relation to peat quality and water regime. *Environmental Monitoring and Assessment*, *188*(12), 655. https://doi.org/10.1007/s10661-016-5669-5

Pádua, L., Marques, P., Hruška, J., Adão, T., Peres, E., Morais, R., & Sousa, J. J. (2018). Multi-temporal vineyard monitoring through UAV-based RGB imagery. *Remote Sensing*, *10*(12), 1907. https://doi.org/10.3390/rs10121907

Pagano, T., & Sorooshian, S. (2002). Hydrologic cycle. *Encyclopedia of Global Environment Change*.

Painter, T. H., Berisford, D. F., Boardman, J. W., Bormann, K. J., Deems, J. S., Gehrke, F., Hedrick, A., Joyce, M., Laidlaw, R., Marks, D., Mattmann, C., McGurk, B., Ramirez, P., Richardson, M., Skiles, S. M. K., Seidel, F. C., & Winstral, A. (2016). The Airborne Snow Observatory: Fusion of scanning lidar, imaging spectrometer, and physically-based modeling for mapping snow water equivalent and snow albedo. *Remote Sensing of Environment*, *184*(July), 139–152. https://doi.org/10.1016/j.rse.2016.06.018

Pajares, G. (2015). Overview and Current Status of Remote Sensing Applications Based on Unmanned Aerial Vehicles (UAVs). *Photogrammetric Engineering & Remote Sensing*, *81*(4), 281–329. https://doi.org/10.14358/PERS.81.4.281

Perich, G., Hund, A., Anderegg, J., Roth, L., Boer, M. P., Walter, A., ... & Aasen, H. (2020). Assessment of multi-image unmanned aerial vehicle based high-throughput field phenotyping of canopy temperature. *Frontiers in plant science*, *11*, 150. https://doi.org/10.3389/fpls.2020.00150

Prokop, A. (2008). Assessing the applicability of terrestrial laser scanning for spatial snow depth measurements. *Cold Regions Science and Technology*, *54*(3), 155–163. https://doi.org/10.1016/j.coldregions.2008.07.002

Prokop, A., Schirmer, M., Rub, M., Lehning, M., & Stocker, M. (2008). A comparison of measurement methods: Terrestrial laser scanning, tachymetry and snow probing for the determination of the spatial snow-depth distribution on slopes. *Annals of glaciology*, *49*, 210–216.

Purinton, B., & Bookhagen, B. (2019). *Introducing PebbleCounts: A grain-sizing tool for photo surveys of dynamic gravel-bed rivers*. https://doi.org/10.5194/esurf-2019-20

Qin, D., Yao, T., Ding, Y., & Ren, J. (2021). *Introduction to Cryospheric Science*. Springer Nature.

Raghavendra, N. S., & Deka, P. C. (2016). Multistep Ahead Groundwater Level Time-Series Forecasting Using Gaussian Process Regression and ANFIS. In R. Chaki, A. Cortesi, K. Saeed, & N. Chaki (Hrsg.), *Advanced Computing and Systems for Security: Volume 2* (S. 289–302). Springer India. https://doi.org/10.1007/978-81-322-2653-6_19

Rahimzadeh-Bajgiran, P., Berg, A. A., Champagne, C., & Omasa, K. (2013). Estimation of soil moisture using optical/thermal infrared remote sensing in the Canadian Prairies. *ISPRS Journal of Photogrammetry and Remote Sensing*, *83*, 94–103. https://doi.org/10.1016/j.isprsjprs.2013.06.004

Rahman, M. M., McDermid, G. J., Strack, M., & Lovitt, J. (2017). A New Method to Map Groundwater Table in Peatlands Using Unmanned Aerial Vehicles. *Remote Sensing*, *9*(10), 1057.

https://doi.org/10.3390/rs9101057

Rasul, G., & Molden, D. (2019). The global social and economic consequences of mountain cryospheric change. *Frontiers in Environmental Science*, *7*, 91.

Regan, S., Flynn, R., Gill, L., Naughton, O., & Johnston, P. (2019). Impacts of Groundwater Drainage on Peatland Subsidence and Its Ecological Implications on an Atlantic Raised Bog. *Water Resources Research*, *55*(7), 6153–6168. https://doi.org/10.1029/2019WR024937

Remondino, F., Barazzetti, L., Nex, F., Scaioni, M., & Sarazzi, D. (2011). *UAV PHOTOGRAMMETRY FOR MAPPING AND 3D MODELING – CURRENT STATUS AND FUTURE PERSPECTIVES –. XXXVIII*(September), 14–16.

Remondino, F., Spera, M. G., Nocerino, E., Menna, F., & Nex, F. (2014). State of the art in high density image matching. *The photogrammetric record*, *29*(146), 144–166.

Reus, M. (2022). *Evaluation of Global Soil Moisture Products for Local Scale Applications*.

Revuelto, J., Alonso-Gonzalez, E., Vidaller-Gayan, I., Lacroix, E., Izagirre, E., Rodríguez-López, G., & López-Moreno, J. I. (2021). Intercomparison of UAV platforms for mapping snow depth distribution in complex alpine terrain. *Cold Regions Science and Technology*, *190*, 103344. https://doi.org/10.1016/j.coldregions.2021.103344

Rhee, D. S., Kim, Y. D., Kang, B., & Kim, D. (2017). Applications of unmanned aerial vehicles in fluvial remote sensing: An overview of recent achievements. *KSCE Journal of Civil Engineering*, *2*(22), 588–602. https://doi.org/10.1007/s12205-017-1862-5

Ribeiro-Gomes, K., Hernández-López, D., Ortega, J. F., Ballesteros, R., Poblete, T., & Moreno, M. A. (2017). Uncooled Thermal Camera Calibration and Optimization of the Photogrammetry Process for UAV Applications in Agriculture. *Sensors*, *17*(10), Article 10. https://doi.org/10.3390/s17102173

Rubin, D. M. (2004). A Simple Autocorrelation Algorithm for Determining Grain Size from Digital Images of Sediment. *Journal of Sedimentary Research*, *74*(1), 160–165. https://doi.org/10.1306/052203740160

Rubio, E., Caselles, V., & Badenas, C. (1997). Emissivity measurements of several soils and vegetation types in the 8–14, μm Wave band: Analysis of two field methods. *Remote Sensing of Environment*, *59*(3), 490–521. https://doi.org/10.1016/S0034-4257(96)00123-X

Salehi Hikouei, I., Kim, S. S., & Mishra, D. R. (2021). Machine-Learning Classification of Soil Bulk Density in Salt Marsh Environments. *Sensors*, *21*(13), Article 13. https://doi.org/10.3390/s21134408

Sankey, T. T., Donager, J., McVay, J. L., & Sankey, J. B. (2017). UAV lidar and hyperspectral fusion for forest monitoring in the southwestern USA. In *Remote Sensing of Environment* (Bd. 195, S. 3043). https://doi.org/10.1016/j.rse.2017.04.007

Scherrer, D., & Körner, C. (2011). Topographically controlled thermal-habitat differentiation buffers alpine plant diversity against climate warming. *Journal of Biogeography*, *38*(2), 406–416. https://doi.org/10.1111/j.1365-2699.2010.02407.x

SCHUMM, S. A., & Khan, H. (1972). Experimental study of channel patterns. *Geological Society of America Bulletin*, *83*(6), 1755–1770.

Serafin, A., Pogorzelec, M., & Bronowicka-Mielniczuk, U. (2023). The Influence of Shallow Peatland Water Quality on Characteristics of the Occurrence of Selected Herb Species in the Peatlands of Eastern Poland. *International Journal of Environmental Research and Public Health*, *20*(4), 2788.

Sharma, B., Kumar, J., Ganguly, A. R., & Hoffman, F. M. (2022). Carbon Cycle Extremes Accelerate Weakening of the Land Carbon Sink in the Late 21st Century. *Biogeosciences Discussions*, 1–21. https://doi.org/10.5194/bg-2022-178

Shaw, J., Nugent, P., Pust, N., Thurairajah, B., & Mizutani, K. (2005). Radiometric cloud imaging with an uncooled microbolometer thermal infrared camera. *Optics Express*, *13*(15), 5807–5817. https://doi.org/10.1364/opex.13.005807

Silva, L., Conceição, L. A., Lidon, F. C., & Maçãs, B. (2023). Remote Monitoring of Crop Nitrogen Nutrition to Adjust Crop Models: A Review. *Agriculture*, *13*(4), Article 4. https://doi.org/10.3390/agriculture13040835

Singh, K. K., & Frazier, A. E. (2018). A meta-analysis and review of unmanned aircraft system (UAS) imagery for terrestrial applications. *International Journal of Remote Sensing*, *39*(15–16), 5078–5098.

Smith, E. P. (1998). Randomization methods and the analysis of multivariate ecological data. *Environmetrics*, *9*(1), 37–51. https://doi.org/10.1002/(SICI)1099-095X(199801/02)9:1<37::AID-ENV284>3.0.CO;2-T

Steenvoorden, J., Limpens, J., Crowley, W., & Schouten, M. G. C. (2022). There and back again: Forty years of change in vegetation patterns in Irish peatlands. *Ecological Indicators*, *145*, 109731. https://doi.org/10.1016/j.ecolind.2022.109731

Stevenson, J. D., O'Young, S., & Rolland, L. (2015). Beyond Line of Sight Control of Small Unmanned Aerial Vehicles Using a Synthetic Environment to Augment First Person Video. *Procedia Manufacturing*, *3*, 960–967. https://doi.org/10.1016/j.promfg.2015.07.146

Stigter, E. E., Steiner, J. F., Koch, I., Saloranta, T. M., Kirkham, J. D., & Immerzeel, W. W. (2021). Energy and mass balance dynamics of the seasonal snowpack at two high-altitude sites in the Himalaya. *Cold Regions Science and Technology*, *183*, 103233.

Still, C., Powell, R., Aubrecht, D., Kim, Y., Helliker, B., Roberts, D., Richardson, A. D., & Goulden, M. (2019). Thermal imaging in plant and ecosystem ecology: Applications and challenges. *Ecosphere*, *10*(6), e02768. https://doi.org/10.1002/ecs2.2768

Suter, S., & Hoelzle, M. (2002). Cold firn in the Mont Blanc and Monte Rosa areas, European Alps: Spatial distribution and statistical models. *Annals of Glaciology*, *35*, 9–18.

Tahir, M. N., Naqvi, S. Z. A., Lan, Y., Zhang, Y., Wang, Y., Afzal, M., ... & Amir, S. (2018). Real time estimation of chlorophyll content based on vegetation indices derived from multispectral UAV in the kinnow orchard. *International Journal of Precision Agricultural Aviation*, *1*(1). https://doi.org/10.33440/j.ijpaa.20180101.0001

Tilahun, T., & Seyoum, W. M. (2021). High-Resolution Mapping of Tile Drainage in Agricultural Fields Using Unmanned Aerial System (UAS)-Based Radiometric Thermal and Optical Sensors. *Hydrology*, *8*(1), Article 1. https://doi.org/10.3390/hydrology8010002

Titus, T. N., Wynne, J. J., Jhabvala, M. D., & Cabrol, N. A. (2022). Using near–surface temperature data to vicariously calibrate high-resolution thermal infrared imagery and estimate physical surface properties. *MethodsX*, *9*, 101644. https://doi.org/10.1016/j.mex.2022.101644

Tmušić, G., Manfreda, S., Aasen, H., James, M. R., Gonçalves, G., Ben-Dor, E., Brook, A., Polinova, M., Arranz, J. J., Mészáros, J., Zhuang, R., Johansen, K., Malbeteau, Y., de Lima, I. P., Davids, C., Herban, S., & McCabe, M. F. (2020). Current Practices in UAS-based Environmental Monitoring. *Remote Sensing*, *12*(6), Article 6. https://doi.org/10.3390/rs12061001

Torres-Sánchez, J., López-Granados, F., De Castro, A. I., & Peña-Barragán, J. M. (2013). Configuration and Specifications of an Unmanned Aerial Vehicle (UAV) for Early Site Specific Weed Management. *PLoS ONE*, *8*(3). https://doi.org/10.1371/journal.pone.0058210

Triggs, B., McLauchlan, P. F., Hartley, R. I., & Fitzgibbon, A. W. (2000). *Bundle adjustment—A modern synthesis*. 298–372.

Turetsky, M. R., Benscoter, B., Page, S., Rein, G., Van Der Werf, G. R., & Watts, A. (2015). Global vulnerability of peatlands to fire and carbon loss. *Nature Geoscience*, *8*(1), 11–14.

Turpie, K. R. (2013). Explaining the Spectral Red-Edge Features of Inundated Marsh Vegetation. *Journal of Coastal Research*, *29*(5), 1111–1117. https://doi.org/10.2112/JCOASTRES-D-12-00209.1

Vander Jagt, B. J., Durand, M. T., Margulis, S. A., Kim, E. J., & Molotch, N. P. (2015). On the characterization of vegetation transmissivity using LAI for application in passive microwave remote sensing of snowpack. *Remote Sensing of Environment*, *156*, 310–321. https://doi.org/10.1016/j.rse.2014.09.001

Varhola, A., Coops, N. C., Weiler, M., & Moore, R. D. (2010). Forest canopy effects on snow accumulation and ablation: An integrative review of empirical results. *Journal of Hydrology*, *392*(3–4), 219–233. https://doi.org/10.1016/j.jhydrol.2010.08.009

Vautherin, J., Rutishauser, S., Schneider-Zapp, K., Choi, H. F., Chovancova, V., Glass, A., & Strecha, C. (2016). Photogrammetric Accuracy and Modeling of Rolling Shutter Cameras. *ISPRS Annals of*

Photogrammetry, Remote Sensing and Spatial Information Sciences, *III3*, 139–146. https://doi.org/10.5194/isprs-annals-III-3-139-2016

Wagner, B., & Egerer, M. (2022). Application of UAV remote sensing and machine learning to model and map land use in urban gardens. *Journal of Urban Ecology*, *8*(1), juac008. https://doi.org/10.1093/jue/juac008

Wang, C., & Myint, S. W. (2015). A Simplified Empirical Line Method of Radiometric Calibration for Small Unmanned Aircraft Systems-Based Remote Sensing. *IEEE Journal of Selected Topics in Applied Earth Observations and Remote Sensing*, *8*(5), 1876–1885. https://doi.org/10.1109/JSTARS.2015.2422716

Wehrhan, M., Rauneker, P., & Sommer, M. (2016). UAV-Based Estimation of Carbon Exports from Heterogeneous Soil Landscapes—A Case Study from the CarboZALF Experimental Area. *Sensors*, *16*(2), Article 2. https://doi.org/10.3390/s16020255

Wever, N., Fierz, C., Mitterer, C., Hirashima, H., & Lehning, M. (2014). Solving Richards Equation for snow improves snowpack meltwater runoff estimations in detailed multi-layer snowpack model. *The Cryosphere*, *8*(1), 257–274.

Wierzbicki, D. (2017). Determination of Shift/Bias in Digital Aerial Triangulation of UAV Imagery Sequences. *IOP Conference Series: Earth and Environmental Science*, *95*(3), 032033. https://doi.org/10.1088/1755-1315/95/3/032033

Wigmore, O., Mark, B., McKenzie, J., Baraer, M., & Lautz, L. (2019). Sub-metre mapping of surface soil moisture in proglacial valleys of the tropical Andes using a multispectral unmanned aerial vehicle. *Remote Sensing of Environment*, *222*, 104–118. https://doi.org/10.1016/j.rse.2018.12.024

Xu, J., Morris, P. J., Liu, J., & Holden, J. (2018). PEATMAP: Refining estimates of global peatland distribution based on a meta-analysis. *CATENA*, *160*, 134–140. https://doi.org/10.1016/j.catena.2017.09.010

Yan, H., Wang, S. Q., Billesbach, D., Oechel, W., Zhang, J. H., Meyers, T., Martin, T. A., Matamala, R., Baldocchi, D., Bohrer, G., Dragoni, D., & Scott, R. (2012). Global estimation of evapotranspiration using a leaf area index-based surface energy and water balance model. *Remote Sensing of Environment*, *124*, 581–595. https://doi.org/10.1016/j.rse.2012.06.004

Yu, B., & Kumbier, K. (2017). Artificial Intelligence and Statistics. *arXiv preprint arXiv:1712.03779*.

Zheng, Z., Ma, Q., Qian, K., & Bales, R. C. (2018). Canopy Effects on Snow Accumulation: Observations from Lidar, Canonical-View Photos, and Continuous Ground Measurements from Sensor Networks. *Remote Sensing*, *10*(11), Article 11. https://doi.org/10.3390/rs10111769